Modelling and Control of Object Handover,

A Study in Human-Robot Interaction

BY

MOHAMMAD SINA PARASTEGARI
M.Sc., University of Tehran, 2012
B.Sc., Isfahan University of Technology, 2009

THESIS

Submitted as partial fulfillment of the requirements
for the degree of Doctor of Philosophy in Electrical and Computer Engineering
in the Graduate College of the
University of Illinois at Chicago, 2018

Chicago, Illinois

Defense Committee:

Miloš Žefran, Chair and Advisor
Mojtaba Soltanalian
Jim Patton, Bioengineering
Brian Ziebart, Computer Science
Max Berniker, Mechanical & Industrial Engineering

to Shantia, the love of my life

and my parents, to whom I owe the most

ACKNOWLEDGMENTS

I would like to thank my adviser Prof. Miloš Žefran, for his great support. It has been an honor to be his student. I appreciate his time, ideas and leadership that guided me through my research and made my PhD study a productive, enjoyable experience.

Besides my adviser, I would like to thank Dr. Ehsan Noohi, for his insightful comments and encouragement. He has been a great mentor to me who always pushed me forward.

I thank my fellow labmates Bahareh Abbasi, Yao Feng, Maria Javaid, Andrey Yavolovsky, Sima Behpour and Wen Jiang for the productive discussions and for all the fun we had in the last four years.

Last but not the least, I would like to thank my parents, and my brother and my two sisters for supporting me spiritually during my study. And most of all, to my wife Shantia, who has been truly patient and encouraging during all these years: thank you, it would not be possible without your unconditional support.

SP

CONTRIBUTION OF AUTHORS

Parts of Chapter 3 has been published in Parastegari *et al.* [1]. Miloš Žefran, my adviser, was the lead investigator in this project. I was responsible for the idea of failure-recognition, designing and implementation of the fail-safe handover controller. Ehsan Noohi contributed in developing the idea and also in editing the manuscript and Bahareh Abbasi contributed in conducting the human study.

TABLE OF CONTENTS

TABLE OF CONTENTS (Continued)

LIST OF TABLES

LIST OF FIGURES

LIST OF FIGURES (Continued)

LIST OF FIGURES (Continued)

FIGURE **PAGE**

SUMMARY

Object handover is a common physical interaction between humans. It is thus also of significant interest for human-robot interaction. In this work, we are focused on robot-to-human object handover. To implement the task on the robot, the configuration (position and orientation) in which the object is transferred should be selected so that the handover is safe and comfortable for the human. The trajectory along which the robot moves the object to the point of transfer should be also selected so that the robot intention is clear and the handover feels natural to the human. We propose to select the configuration for the transfer and the trajectory to reach this configuration based on what humans do in human-human handover. We describe a human study designed to investigate the human-human handover and propose an ergonomic model that can predict object transfer position observed in the study. A human-robot experiment is then conducted that shows that the proposed model generates transfer positions that match the preferred height and distance relative to the human.

Another significant challenge in robot-to-human handover is how to reduce the failure rate, *i.e.*, ensuring that the object does not fall (object safety), while at the same time allowing the human to easily acquire the object (smoothness). To endow the robot with a failure recovery mechanism, we investigate how humans detect failure during the transfer phase of the handover. We conduct a human study that shows that a human giver primarily relies on vision rather than haptic sensing to detect the fall of the object. Motivated by this study, a robotic handover system is proposed that consists of a motion sensor attached to the robot's gripper, a force

SUMMARY (Continued)

sensor at the base of the gripper, and a controller that is capable of re-grasping the object if it starts falling. The proposed system is implemented on a Baxter robot and is shown to achieve a smooth and safe handover.

CHAPTER 1

INTRODUCTION

Object handover is a common type of interaction between humans. In a handover, a *giver* hands the object off to a *receiver*. While they both participate in the exchange, they each have a different goal: the giver wants to safely release the object while the receiver wants to readily acquire the control of the object and establish a stable grasp [4]. Different characteristics of human-human handovers have been studied in the literature. Shibata *et al.* analyzed the human hand trajectory during the task [5], Basili *et al.* studied reaching motion of humans [6] and Mason *et al.* investigated grip forces applied to the object by the giver and the receiver [4].

The handover task has attracted much attention from human-robot interaction community in an effort to equip assistive robots with a similar functionality. There are variety of applications for robots that can deliver objects to humans, *e.g.*, a helper robot that can assist a mechanic by delivering a tool, or a bartender robot that can deliver your drink. Researchers have studied how to perform human-like handover [7–10] and how to implement smooth and safe robot-to-human handover controllers [3, 11–13].

Strabala *et al.* [14], proposed a structure for robot-to-human object handover consisting of four main steps: *grasping* the object, *approaching* the receiver, *reaching out* and *transferring* the object (See Figure 1). Each phase should be properly planned and executed in order to have a successful handover. There are many questions with regards to each phase that should be answered. For example, the giver should decide how to grasp the object, how to approach

the receiver, when to reach out and where to transfer the object. Answers to these questions determine the *handover configurations*, *i.e.*, the configurations in which the object transfer occurs. While humans habitually select the proper handover configurations, robots have to deliberately select the configurations based on the task conditions.

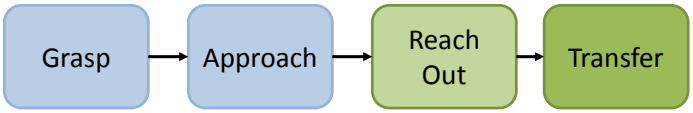

Figure 1. Four main phases of a robot-to-human object handover. In this work, we are focused on the last two phases.

The first step in a robot-to-human handover is for the robot to pick up the object. There are several concerns regarding how to grasp the object for the purpose of a handover: Kim *et al.* [15], investigated the effect of the object's shape on how a robot should grasp an object in order to hand it over to a human. Lopez-Damian *et al.* [16], presented a planner to grasp unknown arbitrary objects for interactive manipulation tasks and Sadigh *et al.* [17], presented a robotic grasping controller that prevents the object slipping while generating minimal normal forces.

After grasping, the next step is to approach the human. Many of the proposed handover controllers for robots are inspired by human-human handovers. Shibata *et al.* [5], analyzed trajectories adopted by humans during the approach phase of a handover. Satake *et al.* [18],

investigated how a robot should approach a human in order to initiate an interaction. Mumm *et al.* [19], studied the relation between human proxemics, that is the amount of space that people need to set between themselves and others, and the robot's likability and eye gaze.

In the Robotics Lab. at the University of Illinois at Chicago, we are mainly focused on physical human-robot interaction. Therefore, in this work we focus on the last two phases of the handover, *i.e.*, the reaching out phase and the transferring phase, where there is a physical interaction between the parties. It is mainly during the reaching out phase that the giver and the receiver coordinate the handover configurations [20]. Many researchers make ad-hoc assumptions on how to select proper handover configurations for a robot-to-human handover. For example, Sisbot *et al.* [8], proposed a manipulation planner that selects the handover configurations by optimizing several cost functions which represent human's safety, visibility and accessibility. While the performance of the proposed planner by Sisbot is evaluated in comparison to a faster shortest path motion, there is no evidence that shows the planner generates natural and intuitive motion. In another study, Cakmak *et al.* [21] investigated human preferences for robot-to-human handover configurations. Subjects are asked to evaluate different handover positions and configurations simulated for the HERB (Home Exploring Robot Butler) robot [22]. The drawback of this approach is that the subjects' lack of experience with HERB robot can result in inaccurate feedback. Asking humans to directly express their preferences in a human-robot interaction is counter intuitive for humans. Take the elderly as an example: while they can clearly express their needs, they cannot determine the details of how an assistive

robot should behave. Another drawback of this study, is that the conclusions can only be applied to HERB robot.

Unlike the study in [21], we propose to obtain preferred handover configurations from human-human handovers. This approach will result in generating human like motions, that will guarantee that the human can interpret the robot intent (*legibility*) and that the motion looks natural. Furthermore, the results can be applied to every manipulator that is capable of grasping and carrying objects. In Chapter 2, we present our study of human-human handovers with the aim of characterizing human preferred handover configurations and we propose a *dyadic joint torque* model to predict the object transfer position in human-human handovers. It is shown that the proposed model is in accordance with the data collected in the human study. Furthermore, through a human-robot experiment, we show that the proposed model can generate object transfer positions at the height favored by humans and with a comfortable distance from the human.

The most critical phase of a handover task is the transfer phase, in which the object load is gradually transferred from the giver to the receiver [2]. The transition starts from the time that the giver makes the decision to open her hand and release the object, and it ends when the object is fully released and the giver is no more in contact with the object. The timing needs to be precisely coordinated between the giver and the receiver. On the giver's side, releasing the object too early may result in the object falling (a failure), while releasing it too late results in high interaction forces [2]. Humans highly benefit from different mechanisms to prevent failure during a handover. Here, we are primarily interested in what the giver can

do. A human giver may attempt to catch the object before it hits the ground. In addition, using social-cognitive reasoning based on haptic information, gaze, the pose of the receiver's body, and the configuration of her hand, humans have a remarkable ability to judge whether the receiver is ready to grasp the object during the handover. In this regard, it is worthwhile noting that while haptic interaction during a handover has been shown to be substantial [2], it mainly happens before the object transfer phase is initiated: if the haptic sensing suggests that there is a problem, the giver will never release the object and there will be no potential failure.

In Chapter 3, we investigate how human givers detect a failure during the transfer phase of the handover. The main question that we want to answer is which sensory modalities are used by human givers to detect a failure? We describe a human study designed to investigate this question. The human study shows that humans primarily rely on vision. That is, they detect the impending fall of the object by observing its motion. This finding is then used to design a robot handover system that consists of a motion sensor attached to the robot's gripper, a force sensor at the base of the gripper, and a controller that is capable of re-grasping the object if it starts falling. We show that the proposed system achieves a safe and smooth handover.

As the final step of our research, in chapter 4, we propose a comprehensive handover system that would manage to execute a sequence of actions in order to perform robot-to-human handover. Safety, smoothness and legibility are achieved using the models presented in Chapters 2 and 3 for the reaching out phase and the transferring phase.

CHAPTER 2

MODELING REACHING OUT PHASE IN OBJECT HANDOVER

Parts of this chapter have been presented in Parastegari et al. [23]. Copyright ©2017, IEEE.

2.1 Introduction

Humans extensively rely on context and communicate through several modalities during the handover [20]. Several previously proposed human-robot handover controllers are inspired by human-human handovers. Kajikawa *et al.* [11] proposed a handover planner that generates human-like motions for the robot and Prada *et al.* [24] used Dynamic Movement Primitives (DMP [25]) to imitate the human motion in handovers.

Different methods have been proposed for planning the reaching out motion. Shibata *et al.* [5], analyzed trajectories adopted by humans while reaching out during a handover. Sisbot *et al.* [7] proposed a planner that generates a safe and legible path for reaching out. Becchio *et al.* [26] compared the velocity profiles for placing an object on a table versus another person's palm. In [27], a robotic handover motion controller is proposed which adapts to sudden movements of the human's hand. Glasauer *et al.* [10] investigated how a robot can convey the intent to hand an object over using reaching out like a human and in [28], different approach directions are compared to find the human-preferred approach direction. In another study, safety and legibility of two different reaching velocity profiles are investigated [29]. Kajikawa *et al.* [30], came up with a controller that selects the velocity of the reaching motion proportional to the

distance to the receiver. In another effort to plan the reaching out motion, Prada *et al.* [24], proposed to use Dynamic Movement Primitives.

Before starting the reaching out motion, the robot should choose the best location and configuration at which the object should be transferred. In [31], a strategy is proposed for the robot to choose the handover location based on the context. In [8], the handover location is chosen based on human's safety, field of view, accessibility and preferences. In [32], it is left up to the human to choose the handover location and the robot simply complies. Aleotti *et al.* [33], proposed a method in which the robot presents the object to the human considering the human preferred way to grasp the object. In [21], five different objects are simulated to find the preferable handover configuration. In another study, affordances are considered when presenting the object to the human [34]. However, there appears to be no work that investigates human preferred handover configurations in human-human handovers. In this chapter, we present our study of human-human handovers with the aim of characterizing human preferred handover configurations. We focus on the reaching phase of handover, *i.e.*, it is assumed that the giver has already grasped the object and approached the receiver, so the giver and the receiver are within a reachable distance from each other. We investigate the giver's velocity during the reaching motion and show that the peak velocity remains unchanged regardless of the task conditions. Furthermore, we propose a *dyadic joint torque* model to predict the object transfer position in human-human handovers and show that the collected data in our human study is in accordance with the proposed model. To evaluate the performance of our model, we implement it on a Baxter robot and conduct a robot-to-human handover experiment. The experimental

results show that the proposed model can generate object transfer positions at the height favored by humans and with a comfortable distance from the human.

2.2 Object Transfer Position in a Handover

An essential part of planning of a handover is to select the object transfer position (P_t). Shibata *et al.* [5] showed that in a handover, the giver traverses a feed-forward minimum-jerk motion to reach P_t and that the giver's motion is started before the receiver begins his/her motion. Shibata suggested it is the giver who selects P_t and dictates it to the receiver. Criteria on selecting P_t include safety, *i.e.*, the position should not cause any harm to the receiver [20], and accessibility, *i.e.*, it should be easy for the receiver to reach and take the object [8]. Here we propose a model to describe the giver's selection of P_t in human-human handovers. Our proposed model predicts P_t based on human ergonomics. There are a large number of studies on human posture modeling based on human ergonomics [35–39]. Katayama *et al.* [35], proposed five different optimization models to characterize human comfort, including the *joint torque model*. Based on this model, the human selects the posture (configuration) that minimizes the following cost function:

$$E_{JT}(q) = \sum_{j=1}^{n} (\tau_j(q))^2 \tag{2.1}$$

where q is the configuration of the arm, τ_j is the joint torque of the jth joint of the arm, and n is the number of joints in the arm. In order to calculate the joint torques, it is necessary to have the dynamical model of the human's arm, including the weight of the links.

The joint torque model and all the other Katayama's optimization models, are designed mainly for single-person manipulation tasks. Here we generalize this model to a dyadic task so it can be used in a handover. We define the *dyadic joint torque* (DJT) cost function, as the sum of the joint torques of the two actors:

$$E_{DJT}(q) = E_{JT}^{giver}(q) + E_{JT}^{receiver}(q) \tag{2.2}$$

where E_{JT}^{giver} and $E_{JT}^{receiver}$ are the giver's and the receiver's cost functions respectively, given by Equation 2.1.

For the sake of simplicity, we make the following assumptions:

1. *Reachable Workspaces*: We assume that the actors are in a close vicinity of each other, so their workspaces mostly overlap.
2. *Plannar Motion*: We assume that the actors are placed in front of each other so that their reaching motion trajectories lie on a vertical plane that includes the actors and P_t (the *Task Plane*) (See Figure 2).
3. *Two Joint Plannar Manipulators*: To further simplify the problem, we model the human's arm as a simple 2-joint plannar manipulator ($n = 2$). The joints are placed at the shoulder and the elbow, and the arm's movement is constrained to the Task Plane.

The *Two Joint Plannar Manipulators* assumption that we made makes it easy to calculate the joint torques for the actors.

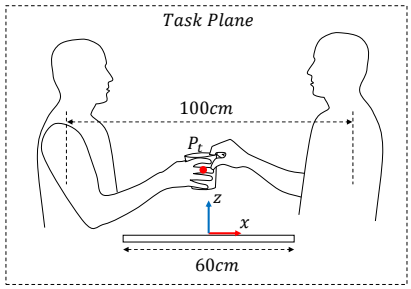

Figure 2. Experimental setup. The *Task Plane* is shown with the object transfer position (P_t) and the coordinate frame. The width of the table and the distance between the actors are $60cm$ and $100cm$ respectively.

The only thing that is left is the weight of the object to be handed over. The weight of the object is mapped to the giver's arm joint torques:

$$T_{obj} = J_{giver}^{T}(q)W_{obj} \tag{2.3}$$

where, W_{obj} is the object's weight force vector, T_{obj} is an 2×1 vector that represents the joint torques caused by W_{obj} and $J_{giver}(q)$ is the giver's arm Jacobian matrix. The reason that we assigned the weight of the object to the giver is that it is the giver who carries the object to the transfer position.

Now, the optimum object transfer position in the *Task Plane* ($\tilde{P}$) can be obtained by minimizing E_{DJT}:

$$\tilde{P} = \arg\min_{q}(E_{DJT}(q)) \tag{2.4}$$

Figure 3 shows an example of the output of the DJT model. In the next section, we present a human study on reaching motion in human-human handovers which validates the proposed model.

2.3 Human Study

To investigate the reaching motion in human-human handovers and validate our proposed model for object transfer position, we conduct a human study with 30 participants (13 females and 17 males) between ages 20 to 39. The participants are recruited from the University of Illinois at Chicago (UIC) students and staff by posting flyers and sending emails to UIC graduate students email-list, according to our approved IRB protocol. The participants perform the handover task with different objects while standing/sitting across a table, where the objects are placed.

2.3.1 Experimental Setup and Procedure

The objects are placed on a table with dimension ($L : 75cm, W : 60cm, H : 70cm$). The position of the participants are specified with two squares marked on the floor. The center of the two squares are at $20cm$ from the opposite edges of the table, which makes a total $100cm$ distance between the two actors in each trial (See Figure 2). At this distance, the workspaces of the subjects have a significant overlap.

To account for the effects of the variations in the properties of the object, *e.g.*, the weight and the shape of the object, we use four different objects that are frequently encountered in daily handovers: a hammer, a knife, an empty cup and a cup full of water (See Figure 4). The empty cup represents an ordinary light-weight object, the hammer represents an object with specific

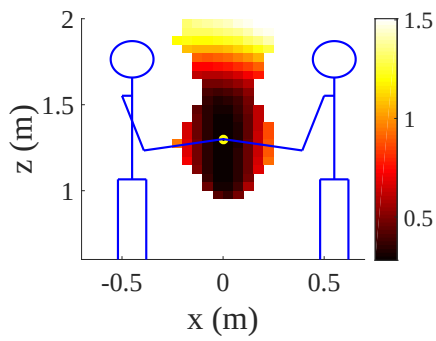

Figure 3. DJT cost function simulated for two actors with $H_i = 187cm$, $L_i = 190cm$ and $W_i = 80Kg$ ($i =$`receiver`,`giver`). The object's weight is $0.2Kg$. The optimum object transfer position is shown by a yellow dot.

shape and functionality, the knife represents an object which requires the giver to be watchful for the safety of the receiver when handing it over, and the cup full of water is an object which requires the giver to be watchful for the safety of the object (the giver might spill the water if moving too fast). To prevent any incident, we made the knife blunt by covering the sharp edge with a thick and transparent tape, so it cannot cut anything. The object type is represented by categorical variable *Obj* that has four levels of (`Hammer`,`Knife`,`EmptyCup`,`FullCup`).

Each pair of participants performs the task in three different poses: (a) both standing; (b) the receiver standing while the giver is sitting; and (c) the giver standing while the receiver is sitting. This is mainly to study the effects of changing the human kinematics on the object transfer position. We do not include the case where both participants are sitting as we expect it to be similar to the both standing case. The pose is described by a categorical variable *Pose* that has three values: (`BothStanding`,`GiverSitting`,`ReceiverSitting`). Each pair performs

Figure 4. Different objects used in the experiment. A hammer, a knife, an empty cup and a cup full of water.

the handover with each object in every possible pose, resulting in a total of 12 handovers per pair of subjects.

Prior to the experiment, the physical dimensions of each subject, including his/her height, arm span and waistline height are measured along with the subject's weight to determine the body kinematics of the subject and the mass of his/her arm. We represent the body dimensions of the subjects by $D_i = \{H_i, L_i, W_i, Wst_i\}$, where $i \in \{giver, receiver\}$ specifies the role, H_i is the height, L_i is the arm span, W_i is the weight and Wst_i is the waistline height of the participant. There are studies such as [40], that relates the length of each link in human's arm to human's height and arm-span. Using this data, we can determine the optimal object transfer position using Equation 2.4 and compare it to the actual measurements.

To track the position of the active hand of the subjects, each trial is recorded by two cameras. One camera is installed on the ceiling to record a top view, and the other one is installed next to the table to record a front view. The cameras are calibrated using finely gridded papers and the

extrinsic parameters of the cameras are extracted by direct linear transformation method [41] to get positioning resolution of about 1.5cm from each camera in the vicinity of the table. Each camera records at 30 frames/sec. The participants are asked to perform the task with their right hand while wearing distinctively colored gloves. The gloves are tracked in the recordings by their color; the center point of the glove is located and considered to be the position of the corresponding hand. Finally, the 2D trajectories extracted from the two cameras are combined to get 3D trajectories with resolution of about 2.0cm in each direction. All the positions are measured in the *reference coordinate frame*, attached to the middle of the table's surface. The reference coordinate frame is shown in Figure 2. The experimental setup and images from the two cameras can be seen in Figure 5.

(a) Front view

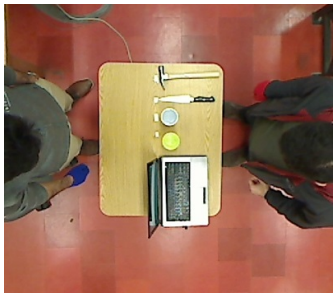

(b) Top view

Figure 5. Experimental setup. The giver is wearing a red glove while the receiver is wearing a blue glove on the right hand.

2.4 Results

2.4.1 Object Transfer Position

In each trial, the subjects hand over one of the four objects, in one of the three poses. We measure the actual object transfer position (P_{t_x}, P_{t_z}) in the task plane and compare it with the predicted position from the model $(\tilde{P}_{t_x}, \tilde{P}_{t_z})$. Figure 6, shows the range of P_t next to the prediction error (err) that is defined as $err = P_t - \tilde{P}_t$, in two directions. While there is a large variation in the measured object transfer position (up to $50cm$), the prediction error is less than $6cm$.

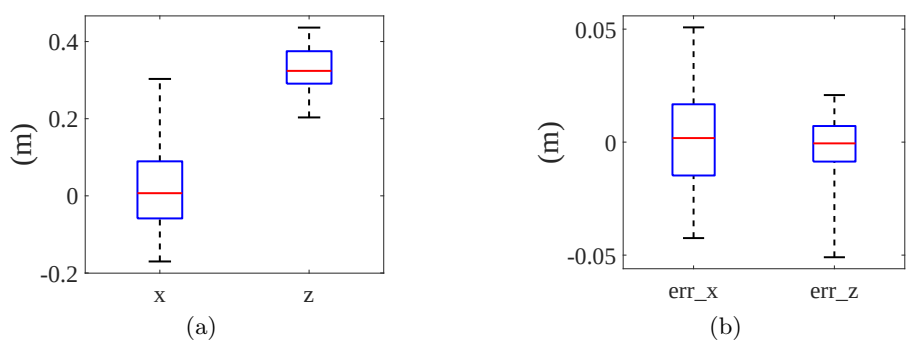

Figure 6. Box plot of (a) the measured object transfer position over all trials, (b) the prediction error. The blue box shows the inter-quartile (25%-75%), the whiskers show min and max, and the red line shows the median of the data.

To statistically evaluate the proposed model, we set up a repeated measures ANOVA test. The within-subject factors include *Obj*, *Pose*, *direction* (1:x, 2:z) and *ActualOrPredicted*

(1: Actual, 2: Predicted). The between-subjects factors are the W_i, H_i and L_i as defined in Section 2.3.1. We have 15 subjects and $4 \times 3 \times 2 \times 2 = 48$ repeated measurements from each subject.

Performing Mauchly's test of sphericity [42] shows that the assumption of sphericity has been violated ($\chi^2(1127) > 10000, p < .0001$). We apply a GreenhouseGeisser correction [43] ($\hat{\varepsilon} = 0.0814$). The repeated measures ANOVA with correction shows significant effect on the measurements from the between-subjects factors: H_{giver} ($F(0.081, 0.1628) = 52.8, p < 0.0185$); $H_{receiver}$ ($F(0.081, 0.1628) = 48.1, p < 0.020$) and L_{giver} ($F(0.081, 0.1628) = 61.7, p < 0.0159$). No significant effect is observed from other between-subjects factors.

To evaluate our model, we perform post-hoc pairwise comparisons. A comparison with Bonferroni correction [44] reveals no difference between P_{t_x} and $\tilde{P}_{t_x}$ ($p = 0.390$) or between P_{t_z} and $\tilde{P}_{t_z}$ ($p = 0.247$). This proves that the prediction of the proposed model is close to the actual measurements.

Another observation is the significant difference in P_{t_x} between two groups of $OBJ =$`FullCup` and $OBJ =$`EmptyCup` ($p < 0.021$). It is shown in Figure 7a, that `EmptyCup` is transferred relatively closer to the receiver compared to `FullCup`. This is consistent with our DJT model that predicts heavier objects are transferred closer to the giver to minimize the joint torques caused by the object's weight.

Furthermore, our data shows that the object is transferred relatively higher in `BothStanding` pose, compared to `GiverSitting` ($p = 0.027$) and `ReceiverSitting` ($p < 0.025$). Figure 7b, clearly shows this difference. This observation can be explained by our DJT model, which

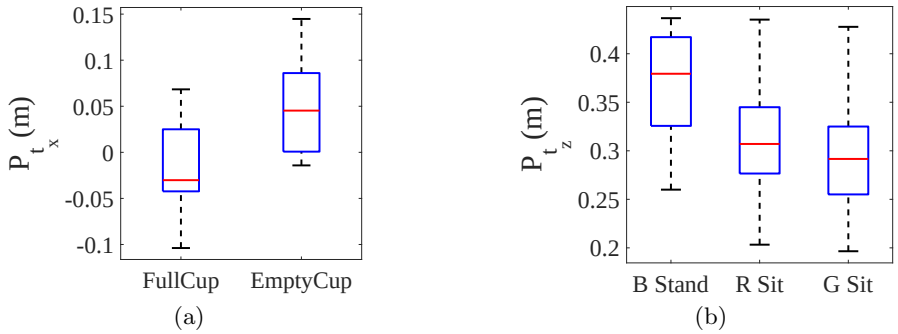

Figure 7. Variations in the object transfer position caused by *Obj* and *Pose*. (a) `FullCup` is transferred farther from the receiver relative to `EmptyCup`; (b) The object is transferred at relatively higher position in `BothStanding` pose compared to the two other poses. The blue box shows the inter-quartile (25%-75%), the whiskers show min and max, and the red line shows the median of the data.

predicts lower object transfer position when one of the actors is sitting, to decrease the generated joint torques for that actor.

2.4.2 Reaching Motion

We computed the absolute velocity of motion for both the giver and the receiver from the time that the giver grasps the object to the time that the object is transferred. Figure 8, shows a histogram of the velocity profiles, normalized in terms of duration and the peak value. It is clearly shown that the velocities have a bell-shaped profile. This is consistent with the results of Shibata's study [5] that shows the giver and the receiver both traverse a minimum-jerk trajectory to reach the object transfer position.

Figure 8a, shows that the normalized giver's velocity of reaching motion has a bell-shaped profile. Note that the actual velocity profile has a duration and a peak value. The duration

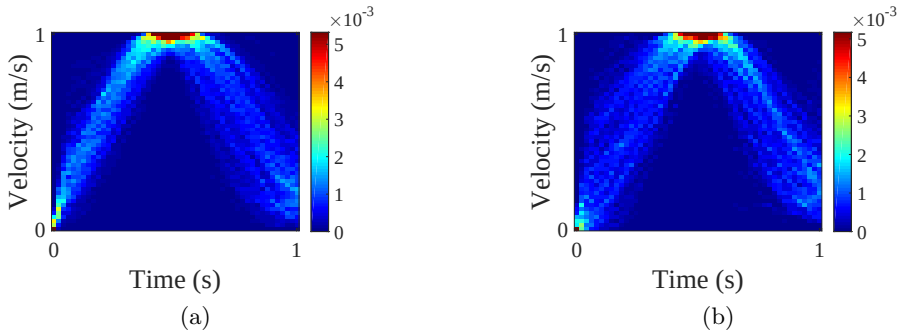

Figure 8. Histogram of normalized velocity of motion for (a) giver, (b) receiver.

of the reaching motion is related to the distance between the actors and the object transfer position that we studied in Section 2.4.1. Here, we focus on the peak velocity of the giver's reaching motion. In order to eliminate the effect of the distance, we normalize the velocity by the distance (the area under the velocity curve). We represent the peak value of this normalized velocity by V_{max}.

In our collected data, V_{max} lies between 0.5 $(1/s)$ and 2.7 $(1/s)$. Figure 9, shows the variation in V_{max} in case of different objects and different poses. To study the effects of the task conditions on V_{max}, we set up another repeated measures ANOVA test. The within-subject factors include Obj, $Pose$. We have 15 subjects and $4 \times 3 = 12$ repeated measurements for each subject.

Performing Mauchly's test of sphericity shows that the assumption of sphericity has been violated ($\chi^2(65) > 10000, p < .0001$). We apply a GreenhouseGeisser correction ($\hat{\varepsilon} = 0.2465$). The repeated measures ANOVA with correction shows no significant interaction between Obj and

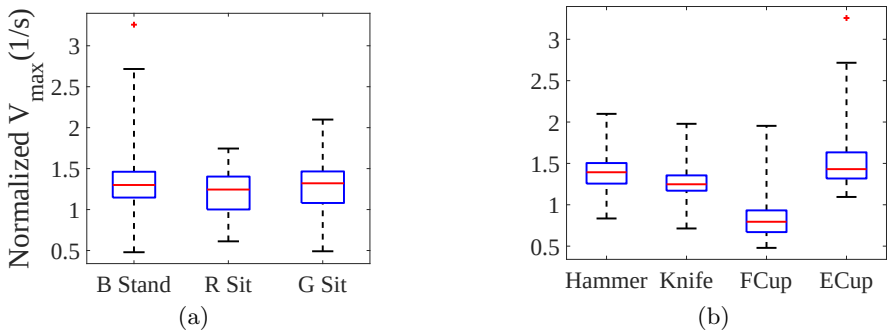

Figure 9. Box plot of normalized V_{max} for (a) different poses and (b) different objects. The `FullCup` is transferred relatively slower than the other objects. The blue box shows the inter-quartile (25%-75%), the whiskers show the data within 5 IQR of the higher and the lower quartiles and the red line shows the median of the data.

Pose ($F(1.479, 20.706) = 0.4884, p = 0.627$). *Obj* has a significant effect on V_{max} ($F(0.739, 10.352) = 18.62, p < 0.001$). However, post-hoc pairwise comparisons with Bonferroni correction reveal no significant difference in V_{max} between *Obj*=`Hammer` and *Obj*=`Knife` ($p = 0.3205$); or *Obj*=`Hammer` and *Obj*=`EmptyCup` ($p \simeq 1$); or *Obj*=`Knife` and *Obj*=`EmptyCup` ($p = 0.3854$). In other words, while three of the objects are carried with almost the same velocity, `FullCup` is carried significantly slower. The other factor in the study, *Pose*, shows no significant effect on V_{max} ($F(0.493, 6.902) = 1.9548, p = 0.1987$).

The results of our test on V_{max} suggest that the giver's peak velocity is determined regardless of *Pose*. Also, putting `FullCup` aside, V_{max} remains unchanged for different objects. The conclusion is that the giver's motion has a fixed maximum velocity, regardless of the pose or the object. The only exception is `FullCup`. We speculate that `FullCup` is transferred slower

because of the existing *physical constraint*. In case of a `FullCup`, the giver is aware that moving too fast, he/she might spill the water. Therefore, she selects a lower velocity to be safe.

2.4.3 Other Observations

Grasp configuration: We observed that every giver grasped `Hammer` from the handle and offered the head to the receiver. Also every giver, except one, grasped `Knife` from the handle. That one participant grasped `Knife` from the blade and offered the handle to the receiver. For the cups, we observed that in `GiverSitting` pose, every giver grasped the cups from the side. In the other two poses where the giver is standing, the cups are grasped sometimes from the side and sometimes from the top.

Orientation of the object transfer: Cakmak *et al.* [21] showed that humans tend to maintain the *default orientation* of the object while handing it over. The default orientation of the object is defined as "the orientation in which the object is viewed most frequently in everyday environments". Cakmak argues that the reason behind it is to maintain the object main functionality [21].

In our experiment, any upright orientation is considered a default orientation for `EmptyCup` and `FullCup`. For `Knife` and `Hammer`, the default orientation is lying with the handle toward the giver. Our data shows that the subjects almost always maintain the default orientation, except when they are transferring `Knife`. Our recordings show that the giver tilts `Knife` either to the right (51% of the trials), to the left (13% of the trials), or to the top (22% of the trials) so the sharp edge does not threaten the receiver. In 13% of the trials, `Knife` is transferred in default orientation. We speculate that humans prefer to preserve the main functionality of the

object, unless the main functionality can be harmful to the receiver. In this case, the giver changes the orientation of the object in order to prevent any incident.

2.5 Human Robot Experiment

Based on the results of Shibata's study [5], we know that in human-human handovers, it is the giver who selects the position of the object transfer and dictates it to the receiver. Our DJT model suggests that the giver considers the comfort of both herself, and the receiver, when selecting the optimum object transfer position. Now the question is, can we apply the DJT model to a robot giver in a robot to human handover? If yes, what is the best policy for the robot? Does the robot have to maximize the comfort for both the receiver and itself? Or should it be just the comfort of the receiver?

Most of the assistive robots have dimensions bigger than humans. For the motion of the robot to be natural, we propose to replace the robot's kinematics in our DJT model with kinematics from one tall stout human. This results in the robot's motion to be similar to what the human receiver expects to see from a human with the similar physical dimensions to the robot. In order to evaluate the performance of the model in this case, we perform a human-robot experiment in which the robot plays the role of a giver in a handover task. Our experiment shows that in terms of the height above the ground, the subjects prefer the object transfer position generated by our DJT model to alternative positions. In terms of the distance from the human, there is no significant preference between the position generated by DJT model and one alternative position.

2.5.1 Experimental Setup and Procedure

Ten people between ages 23 to 29 participated in our experiment (2 females and 8 males). The participants were recruited in the same way we recruited the participants in the human study (see Section 2.3). The height, weight, arm span and waistline height of each subject were measured prior to the experiment.

We implemented our model on a Baxter Robot [45] with an electrical 2-finger gripper. There is a table with dimension ($L : 75cm, W : 60cm, H : 70cm$) at a distance of $40cm$ in front of the robot. In each trial, the robot grasps an object that is placed on the table, reaches out to the human subject and transfers the object to the human. The subject is sitting/standing across the table at a distance of $20cm$ from the edge of the table. The robot releases the object when the subject applies a pulling force to the object. To measure the applied force, a SI-65-5 ATI Gamma force sensor [46] is added to the robot's arm, between the end-effector and the gripper, through two 3D-printed interfaces. The force sensor output is sampled at 100Hz and the data is transferred to a PC through a PCI-6034 NI data acquisition board [47]. Figure 10, shows the robot's arm, the gripper and the force sensor.

To get familiar with the robot, each participant performs the handover task, receiving an empty cup from the robot, 2 times while the subject is standing, and 2 times while the subject is sitting on a chair across the table. After this, each participant performs four different tasks:

1. In the first task, the subject stands across the table, in front of the robot. The robot passes an object (an empty cup with weight=$65 \pm 5g$) to the participant in four different locations (P_1 to P_4). P_1 is selected by the DJT model. Two other positions are selected

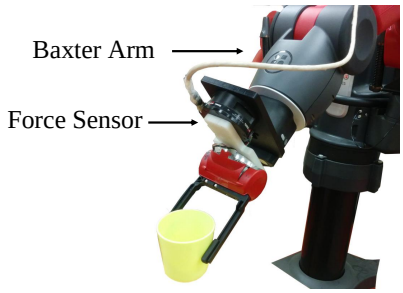

Figure 10. Experimental setup. A force sensor is installed between the Baxter's end-effector and the electrical gripper.

at the same height as P_1, but $15cm$ farther from the receiver (P_2), and $15cm$ closer to the receiver (P_3). P_4 is selected $15cm$ below P_1, at the same distance from the receiver (see Figure 11). P_1 to P_4 are selected by the robot in a randomized order to make sure that the results do not depend on the order. The subject is asked to compare the four object transfer positions.

2. In the second task, the subject sits on a chair across the table, in front of the robot. Again, the robot passes an object (the same empty cup as in task 1) to the participant in four different locations (P_1 to P_4). P_1 is selected by the DJT model. Two other positions are selected at the same height as P_1, but $15cm$ farther from the receiver (P_2), and $15cm$ closer to the receiver (P_3). This time, P_4 is selected $15cm$ above P_1, at the same distance from the receiver. P_1 to P_4 are selected by the robot in a randomized order, to make sure that the results do not depend on the order. The subject is asked to compare the four object transfer positions.

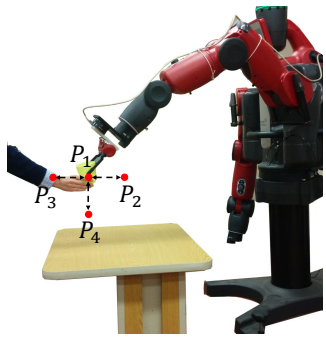

Figure 11. Different object transfer positions in task 1 of our human-robot experiment. The human is standing behind the table in this task.

3. In the third task, the robot hands over a heavy object (a cup full of water with weight $= 335 \pm 5g$) in two different locations (P_1 and P_2) while the subject is sitting behind the table. P_1 is selected by the DJT model. P_2 is a location simulated by the DJT model for a hypothetical light object (the same empty cup as in task 1).

4. In the forth task, the robot hands over a light object (the same empty cup as in task 1) at the same two locations as in task 3.

In our DJT model, the dimensions of the robot are replaced by dimensions of a human with height=190cm, weight=100Kg and arm-span=200cm. After completing each task, the subject is asked to answer a questionnaire that compares different object transfer positions:

1. *Preference*: Which trial did you prefer?

2. *Naturalness*: Which trial looked more natural?

The subjects can choose any one of the trials, more than one trial, or "all were the same" as an answer to each question. For each position, an overall score is calculated in each question, that is equal to the number of times that position is selected by one of the subjects.

2.5.2 Results

Table I, shows the score of each position in each task. In task 1, P_1 is preferred by significantly more participants than P_4 ($t = 2.63, p = 0.0251$). That shows the generated transfer location by DJT model is at the preferred height. P_1 also looked more natural to significantly more subjects compared to P_4 ($t = 2.61, p = 0.0261$). At the same time, there is no significant preference for P_1 over P_3 ($t = -0.49, p = 0.63$). These two locations are different in terms of the distance to the receiver.

Results of task 2, similar to task 1, show that the transfer location generated by the DJT model is at the preferred height. P_1 is preferred by significantly more participants ($t = 2.60, p = 0.026$) compared to P_4. P_1 also looked more natural to the subjects compared to P_4 (score 7 to 2), the difference is not significant though. This time also, there is no significant preference for P_1 over P_3 ($t = 0.82, p = 0.42$).

Looking at the results of task 3 and task 4, we see no significant preference for P_1 over P_2 or vice versa, in any of the two tasks (task 3: $t = -0.28, p = 0.78$, task 4: $t = 1.31, p = 0.22$). In the case of a heavy object, P_2 slightly wins the preference score (6 to 5).

Overall, the results of our human-robot experiment validate the DJT model, in terms of the height of the object transfer position generated by the model. At the same time, humans show

TABLE I

HUMAN-ROBOT EXPERIMENT RESULTS: SCORE OF DIFFERENT OBJECT TRANSFER POSITIONS IN EACH TASK

Task #	Criteria	Position			
		P_1 (DJT)	P_2	P_3	P_4
1	Liking	7	1	9	1
	Naturalness	9	1	10	2
2	Liking	8	1	5	1
	Naturalness	7	1	4	2
3	Liking	5	6	-	-
	Naturalness	5	6	-	-
4	Liking	7	3	-	-
	Naturalness	7	3	-	-

no preference for the transfer location generated by DJT model, in terms of the distance from the receiver.

2.6 Discussion

In this chapter, we studied the reaching motion of a human giver in human-human handovers in terms of the selected object transfer position and the velocity of motion. We proposed a dyadic joint torque (DTJ) model to describe how humans choose the object transfer position. We showed that the DTJ model can successfully predict the object transfer position, based on kinematics and body weight of the human actors along with the object's weight. Furthermore, we showed that unless there is a physical constraint, the velocity of the giver's reaching motion does not depend on the object type and/or the actors' pose. At the end, we evaluated our proposed model in a robot-to-human handover experiment and showed that when applied to a

robot giver, our model will select object transfer position at desired height above the ground and comfortable distance from the human.

One possible extension of this work is to investigate the performance of the proposed DJT model, in a *human-to-robot* handover. Predicting the object transfer position is essential in human-to-robot handover: there is no need for online planning for the robot, if a reliable prediction is available. Unlike robot-to-human handover, there are only a few studies regarding the human-to-robot handover in the literature due to the complexity of the object transfer, and lack of reliable human pose detection systems.

CHAPTER 3

FAILURE RECOVERY DURING THE TRANSFER PHASE OF AN OBJECT HANDOVER

Parts of this chapter have been presented in Parastegari et al. [1]. Copyright ©2016, IEEE.

3.1 Introduction

Humans coordinate object transfer by communicating through different channels: verbal communication, vision and most importantly through the sense of touch. It is shown that haptic communication plays an important role in object handover and gives humans the capability of performing efficient handovers without dropping the object [48]. In case that the robot is the giver, there should be an accurate plan about when to open the robot's hand and release the object. Several methods have been proposed regarding this matter: a simple algorithm is to release the object after a predefined period of time [9, 29]. This algorithm frequently fails by dropping the object since there is no coordination between the robot and the receiver. Deyle *et al.* [49] proposed an algorithm in which the robot releases the object once the exerted force to the base of the robot's fingers exceeds a predefined threshold. Bohren *et al.* [50] implemented an impedance controller for the robot, so the object is released whenever the displacement of the robot's hand due to the exerted force by the receiver is more than a certain distance. Another approach proposed by Nagata *et al.* [13] is to continuously check the stable grasp condition.

The object is released once the grasp becomes unstable. This approach requires force/torque sensors at fingertips.

While these approaches focus on a smooth object transfer, they suffer from a high failure rate. A failure happens when the object is dropped during the handover mainly because of a collision with the receiver's hand or an obstacle. Due to such a collision, a similar force or displacement is measured in the robot's hand as if the receiver were pulling the object. So the robot mistakenly releases the object.

In order to make sure that the receiver has fully taken the control of the object before the object is released, the controller's tolerance to disturbances should be increased in these approaches. As a result, a large force must be applied by the receiver to take the object. In other words, there is a trade-off between the handover smoothness and the object safety [3].

In another study, Chan *et al.* [2] investigated the relation between the load forces vs. the grip forces during human-human handovers and showed that the grip force exerted by human givers has a linear relation with the vertical load force they apply. Based on this observation, a human inspired handover controller was proposed and implemented for PR2 robot which shows smooth performance compared to other approaches [3]. While the proposed algorithm is proved to be fail-safe on some level, it only works when the object is transferred in a vertical direction and in quasi-static situation.

In an effort to prevent falling of the object when the object is grasped by a robotic hand, different slip detection and recovery methods have been proposed. Vibration sensing [51], optical tracking of the object [52] and skin-line sensing [53] are among the proposed slip detection

methods. In [54], tactile and force sensors are used to detect a slip. In a study in neurophysiology [55], it is shown that humans detect slippage of objects based on firing activity sensed by high frequency sensors in the finger tips. Once the slip is detected, the grasp force should be regulated to retain the object. Cipriani et el. [56], proposed different hierarchical control strategies to regulate the grasp force and Yussof *et al.* [57], analyzed performance of a tactile based slippage control algorithm for a robotic hand performing grasp-move-twist motion. Although the aforementioned methods effectively improve the safety of the object in a grasp, they cannot be employed in handover, since in the object transfer phase slipping in unavoidable in order to release the object once it is taken by the receiver. The main issue in a handover task is to distinguish between unwanted slippage caused by a collision versus wanted slippage caused by the receiver pulling the object.

In this chapter, we talk about the study that we conducted to investigate the human failure recovery ability during a handover. Our main question was: On which senses do humans rely to detect a failure in a handover? The outcome of the human study shows that humans primarily rely on vision to detect a failure, through watching the object motion. This indicates that information about the object position plays a central role in detecting a fall. However, due to the ready availability of accelerometers, we choose object acceleration as an indicator of the impending fall of the object. This result is used to design a re-grasping mechanism for robots.

The idea of using object acceleration to achieve safer handover has been explored in the past. In [3], the object acceleration is continuously measured and the handover controller ensures that the acceleration is smaller than a threshold before releasing the object. While this method

improves the safety of the handover, it cannot recover from a failure once the object is released, *e.g.*, if the object slips from the receiver's hand. Also, it cannot handle moderate collision between the receiver's hand and the object. In contrast, we propose a handover controller for a two finger robotic gripper that is able to detect and recover from a failure based on the object acceleration. The proposed handover system is implemented on a Baxter Robot and it is shown that it can effectively prevent the object from falling by re-grasping the object when the handover is problematic. Furthermore, it is shown that the proposed controller provides a wide range of angles of pulling for the user and that the user can easily take the object from the robot (compared to existing handover controllers).

3.2 Handover Failure Detection

In a handover, the decision to release the object is made by the giver once she is confident that the receiver has grasped the object or is capable of doing so. The decision is based on the information provided by the sensors, such as vision and haptic sensing, but it is also affected by social-cognitive processes. In [2], it is shown that during the object transfer phase, the object load is gradually transferred from the giver to the receiver. The total duration of the object transfer phase ($t_{transfer}$) is also measured and reported to be between 300ms to 700ms, in an experiment where a baton shaped object with variable weight of 480g to 680g was handed over between the participants. Figure 12 shows a simulation of the forces during the transfer phase of the handover that mimic those presented in [2]. A simple open-loop controller was used to generate the simulation.

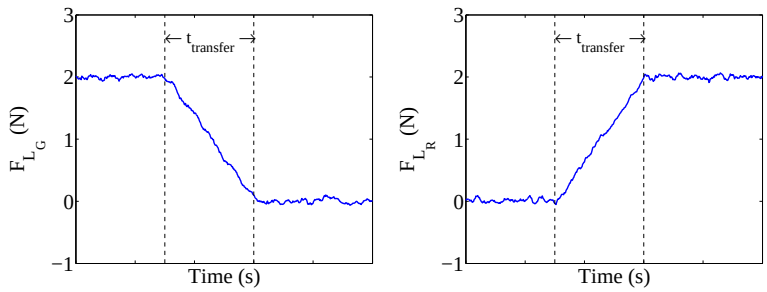

Figure 12. A simulation of the object transfer phase: the object load is gradually transferred from the giver to the receiver during $t_{transfer}$. (a) The giver load force (F_{L_G}). (b) The receiver load force (F_{L_R}). The simulation mimics the forces shown the first panel in Figs. 4 and 5 in [2].

There are different ways a handover can fail. For example, if the giver decides to abort the handover because she determines that the receiver is not ready, this could be considered a failure. In this work, by a *failure* we mean a very specific situation when the giver has made the decision to open her hand and let the object go, but for some reason, the receiver fails to grasp the object so the object starts to fall. In particular, we are interested in how the giver can detect a failure and react to it by re-grasping the object. Our motivation for studying how humans detect failure during the handover is to use what we learn to design a system that allows a robot giver to recover from failures. In particular, we need to determine which sensors should be used by the robot.

We should stress that the focus of our work is on handovers where the forces during the transfer phase follow Figure 12. This happens for instance when the giver holds the object by opposing fingers pressing against vertical faces of the object (see Figure 15). In this case, a

release of the object immediately results in a fall. In other handover configurations, such as when passing a plate to another person, after the giver releases the object, it is still partially supported by her hand so the fall does not happen immediately and there is more time to react to a failure.

The only two senses that might help the giver to detect a failure are vision and haptic sensing (after the fact, a failure can be detected by hearing the object hit the ground; but at that point it is too late to react). Humans can always detect a failure through vision: as they follow the trajectory of the object, if the object is not in the receiver's hand, that means a failure has occured. However, the contribution of haptic sensing is unclear. Haptic sensing is shown to play an important role in object grasping [48] and in particular in slip detection when an object is fully grasped [55]. Slip detection can thus be used to control the grasp [52, 54, 57, 58]. But in a handover, in contrast to grasping, it is expected that the object will slip from the giver's hand as it is transferred from the giver to the receiver so the slip does not indicate a failure. The next section describes a human study that was performed to determine whether humans in the role of a giver use haptic sensing to detect a failure during a handover[1].

3.3 Human Study

The human study is conducted with 10 participants (5 men and 5 women) between ages 21 to 37. The participants are recruited from students and staff at the University of Illinois at Chicago (UIC) by posting flyers and sending emails to UIC graduate students email-list, according to

[1]Clearly, for the receiver, haptic sensing with its ability to detect slip is crucial to securely grasp the object.

our approved IRB protocol. The subjects play the role of the giver in the handover task by keeping an object in their hand. The experimenter plays the role of the receiver and tries to take the object from the subject.

3.3.1 Experimental Setup and Procedure

While blindfolded, each subject performs the handover task 10 times. The object to be handed over is an 8cm×8cm×9.5cm mug (see Figure 13). In each trial, the participant keeps the mug in her hand and the experimenter attempts to take the mug. In half of the trials (5 trials), the experimenter performs the *taking*, *i.e.*, the object is completely grasped using three fingers: the thumb, the index and the middle finger. The mug is then pulled horizontally out of the participant's hand (see Figure 14a, the direction of pulling is shown by a blue arrow). In the other 5 trials, the experimenter performs the *dropping*, *i.e.*, the object is intentionally dropped by putting the index and middle fingers inside the mug and pulling it horizontally (see Figure 14b, the direction of pulling is shown by a blue arrow). In order not to give any clue to the subject, the experimenter tries to touch and pull the mug softly so the participant cannot realize how many fingers are used. The *taking* and *dropping* actions are interleaved randomly so the participant is neither aware of the number of repetitions of each action nor the order of the actions. There is a pillow on the table so in case the object falls, it won't make a loud sound. Also, a loud music is played for the participant through headphones, so she cannot hear the sound of the object hitting the pillow.

The participant's role is to tell whether the object is dropped or taken after each trial. The expectation is that if haptic sensing contributes significantly to detecting a failure during the

transfer by the giver, the participants should be able to detect the drop at a rate significantly better than chance (which would be 50%). Note that the participants are instructed not to re-grasp the object if they feel it was dropped. To determine the effect of the direction of pulling, the experiment is repeated again, but with a different pulling direction. This time, the object is pulled diagonally (see Figures 14c and 14d, the direction of pulling is shown by a red arrow). In total, each subject thus performs 20 trials.

Figure 13. The object and the installed equipment.

In order to maintain the consistency between the trials, we attached a 9 degrees-of-freedom Sensor-Stick SparkFun Inertial Measurement Unit (IMU) [59] to the mug to measure its acceleration (see Figure 13). The IMU is interfaced with a computer through an Arduino MEGA development kit [60]. For each trial, we make sure that the object's acceleration in the direction of pulling falls in the range of 1.5 to 4.5m/s^2; otherwise the trial is disregarded. This range of

accelerations was observed in a pilot study in which several subjects simply handed over the same mug to each other. The object and the IMU weigh 420±10g in total.

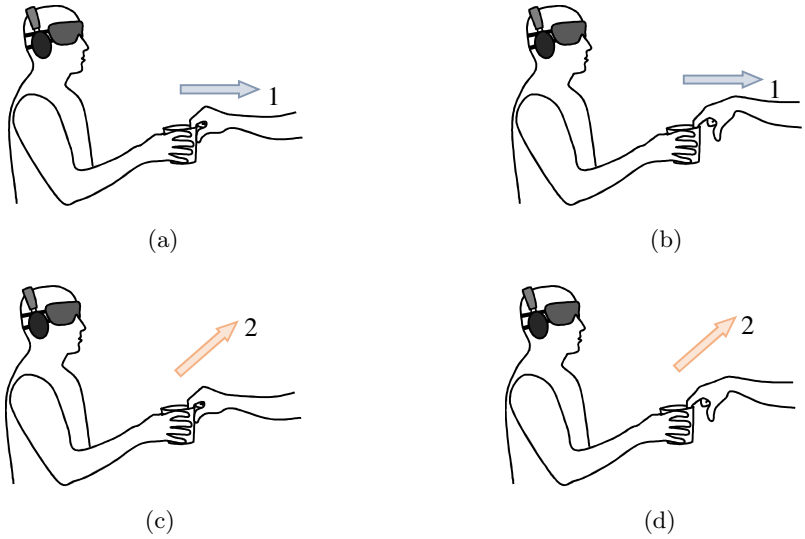

Figure 14. Pulling action in (a) *taking* horizontally, (b) *dropping* horizontally, (c) *taking* diagonally and (d) *dropping* diagonally cases. The blue arrow shows the horizontal pulling direction. The red arrow shows the diagonal pulling direction.

Note that during the human study, several precautions are taken to eliminate the human social-cognitive reasoning that typically takes place during the handover: the experiment is repeated several times in the same configuration and the giver cannot see the experimenter (the receiver) nor her hand.

3.3.2 Results

The range of the magnitudes of the object acceleration in the direction of pulling is shown in Table II. The performance of the participants is summarized in Table III. For example, the first row in Table III indicates that when the experimenter performed the *taking* action and pulled the object horizontally, the success rate was 62%, *i.e.*, in 62% of the trials, participants could correctly identify the action and express that the object was taken. The third row in the table shows that the total success rate of the participants, when the object was pulled horizontally, was 54%. In order to determine the role of haptic sensing, we used the data to test whether or not participants were able to answer correctly significantly more often than chance (50%).

TABLE II

OBJECT ACCELERATION IN THE DIRECTION OF PULLING

Object Acceleration	**Min.** (m/s^2)	**Max.** (m/s^2)	**Ave.** (m/s^2)	**SD** (m/s^2)
Pulling Horizontally	1.6	4.4	3.2	0.7
Pulling Diagonally	1.8	4.4	3.7	0.6

Let $x_i, i = 1, \ldots, 10$, denote the success rate of each participant when the object is pulled horizontally (one sample). The average of all the samples is $\bar{x}_i = 54\%$ and its standard deviation

TABLE III

PERFORMANCE OF THE PARTICIPANTS. PARTICIPANTS WERE INSTRUCTED NOT TO RE-GRASP THE OBJECT IF THEY FELT IT WAS DROPPED.

Pulling Direction	**Action**	**Participant's Guess**	
		Correct	Incorrect
Horizontal	Taking	62%	38%
	Dropping	46%	54%
	Total	***54%***	***46%***
Diagonal	Taking	62%	38%
	Dropping	72%	28%
	Total	***67%***	***33%***

is $SD(x_i) = 13\%$. One-sample t-test indicates that the performance of the participants does not significantly differ from the 50% success rate expected by chance: $t = 0.973, p - value = 0.356$. To make sure that the underlying distribution assumptions of t-test do not affect the analysis, the significance level is also calculated using a non-parametric test. We use a binomial test [61] on the overall success rate of all the participants, tested against a null of 50% success rate. Using binomial test makes sense here because the action is randomly selected in each trial and hence the trials are statistically independent. This test also shows that the success rate does not significantly differ from chance: $p - value = 0.481$. Furthermore, the 95% confidence interval of the success rate is [0.42 , 0.65] which shows that the correct and the incorrect answers are almost equally likely to be selected.

The conclusion is that in this setup, the information provided by haptic sensing is not reliable enough to detect falling of an object during the object transfer phase. In fact, the participants stated that they often could not decide with certainty whether the fall occurred and they just chose a random answer. The performance of participants is slightly improved when the object was pulled diagonally, with participants answering correctly in 67% of trials (row 6 in Table III). We speculate that this improvement is because of the greater difference between the object's motion in *taking* and *dropping* scenarios when the object is pulled diagonally. Even though the success rate in this case is significantly higher than chance ($p - value < 0.01$), the failure rate of 33% is still quite high. Considering that humans can easily detect the failure with their eyes open, the data shows that closing the participants' eyes has significantly affected their performance.

3.4 Robot Handover System with Failure Recovery

Given the results of the human study, we were motivated to choose vision instead of a haptic sensor to detect the fall of the object. In a human-human handover, vision clearly plays a significant role. The giver watches the receiver reaching for the object and perceives her readiness to take it. This information helps the giver to coordinate the time, the location and the configuration of the handover. On the other hand, during the transfer phase, both the giver and the receiver visually monitor the object to ensure the successful completion of the task. However, visual processing is time consuming, both for humans and for computers. In order to use the motion of the object for failure detection, and to allow the robot to react to the failure, motion needs to be monitored with a sensor that has a fast response time.

Among the characteristics of the object's motion, the acceleration can be used as an indicator of an impending fall of the object and this is the modality we used in our work. Object acceleration can be measured by installing an accelerometer on the object; however, this is clearly not a solution that is suitable for implementation on a robot. Instead, the robot should be equipped with a sensor that can measure the object's acceleration with respect to the robot's hand. We propose to attach an optical sensor similar to what is used in an optical mouse, to the finger of the robot. Optical sensors are able to measure acceleration up to 10g [62]. They often have a limited range of operation, *i.e.*, the object should be in close proximity to the sensor (distance<4mm). But in our application in which the object is in contact with the robot's finger, these optical sensors provide a cost-effective and practical solution. Also, like any other position based estimate, our acceleration measurement is subject to high-frequency noise. But in Section 3.5, we show that our proposed controller is highly robust against acceleration measurement noise.

In the following, a model of a handover system with a two finger robotic gripper is proposed. Subsequently, we design a handover controller that includes a re-grasping mechanism. The re-grasping mechanism relies on the feedback that includes the acceleration of the object measured by an optical sensor installed on the gripper, as well as forces measured at the wrist.

3.4.1 System Model

Assume a two finger robotic gripper with an object grasped by the gripper. The robot's wrist is equipped with a force sensor that measures the forces applied to the object and there is an optical sensor attached to the gripper that measures the object acceleration relative to the

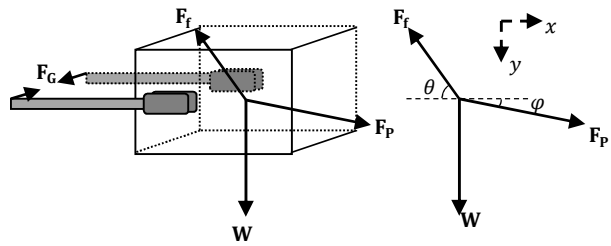

Figure 15. The two finger gripper and applied forces to the object.

gripper. A human subject tries to take the object from the gripper by pulling it. In Figure 15, the gripper, the object and forces applied to the object are shown.

$\mathbf{F_p}$ the pulling force applied by the human, φ is the angle of pulling, $\mathbf{W}$ is the object weight, $\mathbf{F_G}$ is the controlled grip force and $\mathbf{F_f}$ is the friction force between the gripper and the object. For the sake of simplicity, it is assumed that $\mathbf{F_p}$ is in the plane that is perpendicular to the grip force ($\mathbf{F_G}$).

Decomposing applied forces in the x and y directions (see Figure 15), the equations of motion governing the system become:

$$\begin{aligned} F_p \cos\varphi - F_f \cos\theta &= M a_x \\ W + F_p \sin\varphi - F_f \sin\theta &= M a_y \end{aligned} \tag{3.1}$$

where M is the object mass, θ is the angle between the friction force and x axis and a_x and a_y are the components of the object acceleration in the x and y directions, respectively. Italicized letters are used to show scalars including vector norms.

Let F_{sum} be the magnitude of the vector sum of $\mathbf{W}$ and $\mathbf{F_p}$:

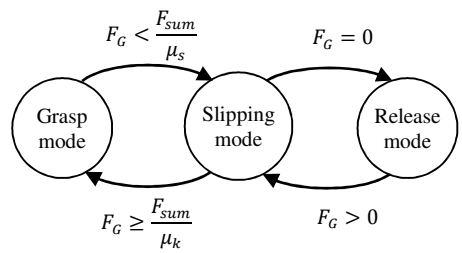

Figure 16. System modes.

$$F_{sum} = \sqrt{(W + F_p \sin\varphi)^2 + (F_p \cos\varphi)^2} \tag{3.2}$$

Based on the configuration of the object and the gripper, the system can be in one of the three modes: the *grasp mode*, the *slipping mode* and the *release mode*. Different system modes and mode switching conditions are shown in Figure 16 and are explained below.

Mode 1 (*Grasp Mode*):

We assume the system starts in the *grasp mode* in which the object is fully grasped and $a_x = a_y = 0$. The human can pull the object but as long as the total external force applied to the object F_{sum} is less than the maximum static friction force ($F_{f_{max}}$), the system stays in the *grasp mode*. We have $F_{f_{max}} = \mu_s F_G$ where μ_s is the static friction coefficient between the object and the gripper (effectively, μ_s is twice the static friction coefficient between the object and each finger of the gripper).

In the *grasp mode* we have:

$$
\begin{aligned}
F_p \cos\varphi &= F_f \cos\theta \\
W + F_p \sin\varphi &= F_f \sin\theta
\end{aligned}
\tag{3.3}
$$

Mode 2 (*Slipping Mode*):

Once F_{sum} exceeds $F_{f_{max}}$, the system switches to the *slipping mode* in which the object slips between the fingers of the gripper. In the *slipping mode*, the system equations become:

$$
\begin{aligned}
F_f &= \mu_k F_G \\
F_p \cos\varphi - F_f \cos\theta &= M a_x \\
W + F_p \sin\varphi - F_f \sin\theta &= M a_y \\
\frac{a_y}{a_x} &= \tan\theta
\end{aligned}
\tag{3.4}
$$

where μ_k is the kinetic friction coefficient between the object and the gripper (twice the kinetic friction coefficient between the object and each finger of the gripper). It is assumed that the object moves in a straight line, so the object's acceleration is in the direction of motion.

While most of the proposed handover controllers in the literature have only two modes of operation (complete grasp and complete release) the *slipping mode* is essential to our controller. In this mode, the object is allowed to move but it is not completely released. Therefore, the object's downward acceleration can be measured and the system can distinguish between an unwanted collision and a force applied by the user. One of our main contributions in this research is to design a controller that keeps the system in the *slipping mode* in order to achieve a smooth and safe handover.

Mode 3 (*release mode*):

Once the output of the controller (F_G) becomes zero, the friction force also becomes zero ($F_f = 0$) and the object is released from the gripper.

3.4.2 Controller Design

We assume that there is a force sensor attached to the robot's wrist that measures the force applied to the object. The output of the force sensor ($\mathbf{F_s}$) is equal to the friction force between the gripper and the object:

$$F_{s_y} = F_f \sin\theta \quad , \quad F_{s_x} = F_f \cos\theta \tag{3.5}$$

In [3], the grip force is chosen based on the vertical load force in a linear fashion ($F_G = \alpha F_{s_y} + F_0$). In this way, the grip force decreases as the user compensates the vertical load force. It is shown in [2] that the grip force must decrease monotonically with the vertical load force in order to achieve a smooth handover. We thus employ the same strategy. But in order to prevent the object from falling, we propose to include the object's downward acceleration in the controller equation. A higher downward acceleration of the object should result in a larger grip force. Also, we want the human to be able to take the object not only vertically, but in any direction. So the x component of the measured force should also be considered. As the x component of the pulling force increases, the grip force should be decreased. Therefore, we propose the controller equation as below:

$$F_G = \alpha F_{s_y} + \beta a_y - \gamma F_{s_x} \tag{3.6}$$

where α, β and γ are constant values. Please note that F_G is bounded below by zero ($F_{G_{min}} = 0$).

According to Equation 3.6, after the object is released from the gripper ($F_{s_x} = F_{s_y} = 0$), even a small value of the object's downward acceleration results in the grip force becoming non-zero, so the system switches back to the *slipping mode*. In order to solve this issue, a $-F_{margin}$ term is added to the controller that makes the system tolerate a small downward acceleration:

$$F_G = \alpha F_{s_y} + \beta a_y - \gamma F_{s_x} - F_{margin} \tag{3.7}$$

It is shown in Section 3.4.4, that F_{margin} helps the stability of the system when the system is in the *release mode*. In discrete time, the controller equation becomes:

$$F_G[n+1] = \alpha F_{s_y}[n] + \beta a_y[n] - \gamma F_{s_x}[n] - F_{margin} \tag{3.8}$$

The control loop is shown in Figure 17. We assume that the dynamics of the gripper is negligible so that the commanded grip force is directly applied to the object. The plant under control consists of the gripper and the object.

The coefficients α, β and γ in Equation 3.8 should be selected properly to achieve the following design goals: (a) the robot should not allow the object to fall; and (b) the handover should happen in a smooth and effortless manner. The following performance and stability conditions should be satisfied in order to achieve the stated design goals.

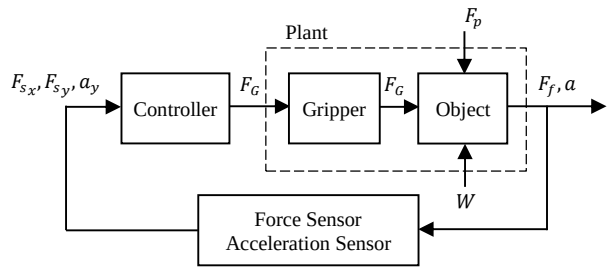

Figure 17. The controller loop.

3.4.3 Performance Conditions

Rest condition: in the *grasp mode*, when the system is at rest ($F_p = 0, a_y = 0, F_{s_y} = W, F_{s_x} = 0$), in order to prevent the object from falling we should have $\mu_s F_G \geq W$. Substituting F_G from Equation 3.7 we have:

$$\alpha \geq \frac{1}{\mu_s} + \frac{F_{margin}}{W} \tag{3.9}$$

Therefore, α should satisfy Equation 3.9 so the object doesn't fall in the *grasp mode*.

Re-grasp Condition: we should make sure that the system switches back from the *release mode* to the *slipping mode* when the object downward acceleration is more than a threshold. In the *release mode* we have $F_{s_x} = F_{s_y} = 0$. Therefore:

$$F_G[n+1] = \beta a_y[n] - F_{margin} \tag{3.10}$$

The maximum object's downward acceleration that the system tolerates is:

$$a_{y_{max}} = \frac{F_{margin}}{\beta} \tag{3.11}$$

In case we have $a_y > a_{y_{max}}$, the system will re-establish the grasp by switching back to the *slipping mode*.

Force overshoot: force overshoot is defined as the pulling force that the user has to apply before the object is released. Here we define the start force threshold F_{ST} as the pulling force that the user has to apply to the object so the system switches from the *grasp mode* to the *slipping mode*. It is shown later that the force overshoot is equal to F_{ST}. To calculate F_{ST} we consider the switching condition from the *grasp mode* to the *slipping mode* at the extreme: $F_{sum} = \mu_s F_G$. Expanding F_{sum} and substituting F_G from Equation 3.7 we have:

$$\sqrt{F_{ST} + W^2 + 2WF_{ST}\sin\varphi} = \mu_s\left[\alpha(W + F_{ST}\sin\varphi) - \gamma(F_{ST}\cos\varphi) - F_{margin}\right] \tag{3.12}$$

Equation 3.12, establishes a relation between the start force threshold and the direction of pulling. In Figure 18, the start force threshold is shown with respect to the pulling angle φ for a specific set of parameters specified in Table IV and three different values of γ.

According to Figure 18, for a specific value of γ, there is a maximum angle (φ_{max}) at which the user can successfully take the object from the robot by pulling it in that direction. For $\gamma = 3$, we have $\varphi_{max} = 20°$. Higher values of γ result in lower start force threshold and wider range of angles at which the user can successfully take the object.

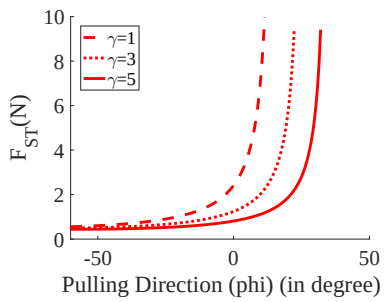

Figure 18. F_{ST} versus the pulling angle φ, plotted for three different values of γ.

TABLE IV

SYSTEM PARAMETERS USED IN THE SIMULATIONS

Parameter	α	β	γ	$F_{margin}(N)$	k_i	$M(Kg)$	μ_s	μ_k
Value	10	3	1	12	0.13	0.2	0.6	0.5

3.4.4 Stability Conditions

Stability of robots physically interacting with humans has been extensively studied [63–69]. The primary focus of these investigations are robots that are physically coupled with humans such as assistive devices and haptic interfaces, where stability is necessary for safety. The common approach in these studies is to model the human (and the environment if needed), either explicitly as an impedance or admittance, or implicitly as a passive subsystem, and the stability of the overall system is then examined.

In tasks such as a handover, it is more accurate to characterize the actions of the human as the exogenous inputs for the robot; the robot needs to generate an appropriate action in

response. As a result, the issue of stability reduces to stability of the robot controllers implementing specific robot actions for arbitrary input.

In the case of the handover, the primary response of the robot is the applied grip force F_G. The stable behavior of the robot thus reduces to two separate conditions: (a) for a constant pulling force F_p (human input), the grip force F_G should converge to a constant; and (b) for a constant pulling force F_p, the system should not switch between different modes (grasp, slipping, release).

Assuming the system is in the *grasp mode*, we can determine F_G by substituting Equation 3.3 and Equation 3.5 into Equation 3.7:

$$F_G = \alpha W + F_p \sin\varphi - \gamma F_p \cos\varphi - F_{margin} \tag{3.13}$$

This shows that in the *grasp mode*, condition (a) is satisfied.

Once the system switches to the sliding mode, it shouldn't switch back to the *grasp mode* unless the pulling force is below F_{ST}. That is to prevent consecutive mode switches. Here we define the stable force threshold (F_{BT}) as the minimum amount of the pulling force that the user has to apply to the object when the system is in the *slipping mode* so the system doesn't switch back to the *grasp mode*. To calculate F_{BT}, we find $\sin\theta$ and $\cos\theta$ from Equation 3.4 and substitute them into Equation 3.5. F_{s_x}, F_{s_y} and a_y can then be found in terms of F_G, F_p and φ:

$$F_{s_y} = \mu_k F_G \frac{W + F_p \sin\varphi}{F_{sum}} \quad , \quad F_{s_x} = \mu_k F_G \frac{F_p \cos\varphi}{F_{sum}}$$
$$a_y = \frac{1}{M}\left(W + F_p \sin\varphi - \mu_k F_G \frac{W + F_p \sin\varphi}{F_{sum}}\right) \tag{3.14}$$

Substituting Equation 3.14 into Equation 3.8 we have:

$$F_G[n+1] = aF_G[n] + b \tag{3.15}$$

where:

$$a = \frac{\mu_k}{F_{sum}} . \left[(W + F_p \sin\varphi)(\alpha - \frac{\beta}{M}) - \gamma F_p \cos\varphi\right] \tag{3.16}$$
$$b = \left[\frac{\beta}{M}(W + F_p \sin\varphi) - F_{margin}\right] \tag{3.17}$$

For Equation 3.15 to be stable and produce bounded output, we should have:

$$|a| \leq 1 \tag{3.18}$$

In other words, the single pole of the system ($z = a$) should be inside the unit circle so the closed loop system becomes stable. Please note that the dynamics of the gripper is neglected. In the extreme case when $|a| = 1$, F_p would be equal to F_{BT}. This gives us F_{BT} as a function of the direction of pulling. In Figure 19a, F_{BT} is shown with respect to pulling angle (φ) for a set of system parameters specified in Table IV. As it is shown in Figure 19a, F_{BT} is greater than

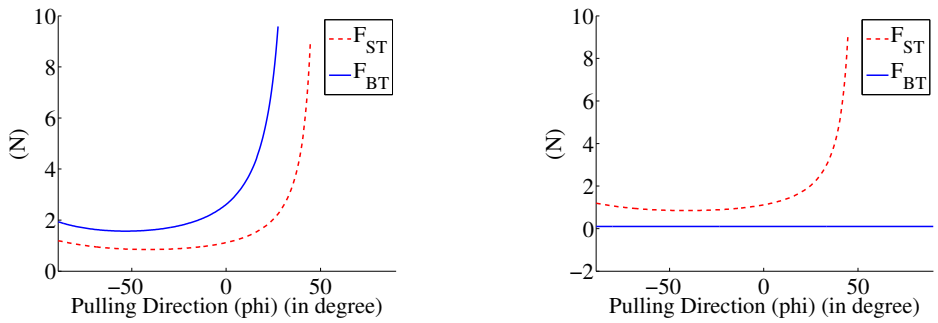

(a) (b)

Figure 19. F_{ST} and F_{BT} with respect to pulling angle φ in (a) the primary controller design and (b) after adding integrator term.

F_{ST}. In fact, it can be shown that the minimum required force to have a stable system is greater than the start force threshold for any set of system parameters. That means, when applying an ascending pulling force, the system switches to the *slipping mode* once F_p exceeds F_{ST} and then switches back to the *grasp mode* before F_p reaches F_{BT}. This results in an unstable situation.

To resolve this issue, we add an integrator term to the system:

$$F_G[n+1] = k_i \left(\alpha F_{s_y}[n] + \beta a_y[n] - \gamma F_{s_x}[n] - F_{margin}\right) + (1-k_i)F_G[n] \tag{3.19}$$

Therefore, Equation 3.16 becomes:

$$a = k_i \frac{\mu_k}{F_{sum}} . \left[(W + F_p \sin\varphi)(\alpha - \frac{\beta}{M}) - \gamma F_p \cos\varphi\right] + (1-k_i) \tag{3.20}$$

Again, we put $|a| = 1$ to calculate F_{BT}. In Figure 19b, F_{BT} and F_{ST} are shown as a function of the pulling direction. Figure 19b shows that the integrator term has pushed the pole of the system inside the unit circle so the system has become stable for all values of the pulling force. It can be shown with further analysis that adding the integrator term not only satisfies ($|a| \leq 1$), but also results in F_G to be descending for a constant pulling force F_p and therefore guarantees the system to stay in the *slipping mode*.

3.5 Simulation Results

Matlab simulations are carried out to evaluate the performance of the controller framework proposed in Section 3.4.2. We define two different actions: (a) *dropping*, and (b) *taking*, similar to what we defined in Section 3.3. In *dropping*, a force is applied to the object, but the weight of the object is not compensated, resulting in the object falling if released by the robot. This is to test whether the robot can prevent a failure. In contrast, in *taking*, it is assumed that the object is taken by a human, so the weight of the object is compensated. In this case, we want to see whether the controller can achieve a smooth handover. The two actions are simulated similarly: in each time step, the pulling force in the desired direction is applied to the object in addition to F_G and W. The acceleration of the object is then calculated considering the friction force between the gripper and the object. The only difference between the two actions is that in a *taking* scenario, the object's weight is canceled out during the transfer phase.

In the simulations, we selected the object's mass $M = 0.2Kg$ and $\mu_s = 0.6$, $\mu_k = 0.5$. The controller parameters are selected as follows: the maximum object's downward acceleration that the system tolerates is set to $4(m/s^2)$. Based on Equation 3.11, β is set to 3 and F_{margin}

is set to 12. Parameter α is then selected equal to 10 to satisfy Equation 3.9. Also, based on Figure 18, γ is set to 5 to achieve $F_{ST}(\varphi = 0) < 1N$, *i.e.*, force overshoot of less than 1N when pulling the object horizontally. The system parameters used in the simulations are summarized in Table IV.

In the first simulation, a horizontal pulling force is applied to the object with $\varphi = 0°$. Both the *dropping* and the *taking* actions are performed. F_p starts from zero at $T_0 = 1s$ and reaches 2N at $T_1 = 1.5s$. In the *dropping* scenario, the pulling force becomes zero again at $T_2 = 2.5s$. In Figures 20a and 20b, the applied pulling force and the controller output are shown for the *taking* and *dropping* actions, respectively. The acceleration of the object for both actions is shown in Figures 20c and 20d. The background colors in the figures indicate the mode of the system: red corresponds to the *grasp mode*, yellow to the *slipping mode*, and green to the *release mode*.

As shown in Figure 20a, in case of *taking*, F_G drops to zero once the pulling force is applied, which means the object is released immediately. Also it is shown in Figures 20b and 20d that while the pulling force is applied, F_G is regulated and a_y is kept below $4m/s^2$. Furthermore, once applying the pulling force stops in Figure 20b, F_G rises back to the initial value, the grasp is re-established and the object's fall is prevented. Another observation is that in Figure 20c, it can be seen that the object briefly accelerates downward before it is completely released. The reason is that we intentionally added a slight delay to the weight compensation algorithm so it better simulates the behavior of a human receiver.

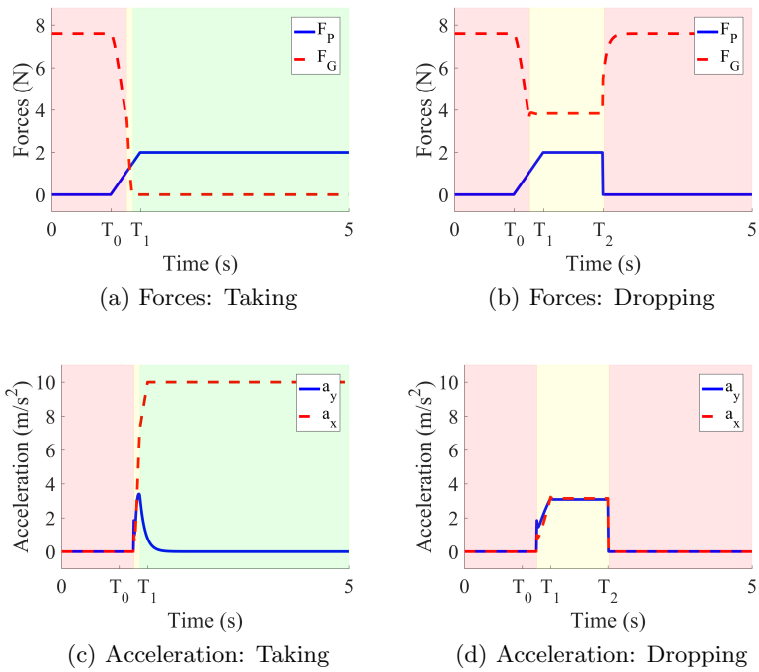

(a) Forces: Taking (b) Forces: Dropping

(c) Acceleration: Taking (d) Acceleration: Dropping

Figure 20. Applied pulling force and grip force in (a) *taking* and (b) *dropping*. Acceleration of the object in (c) *taking* and (d) *dropping*. Red background indicates the *grasp mode*, yellow the *slipping mode* and green the *release mode*.

In the next run, the *taking* action is simulated with two different angles of pulling. In Figures 21a and 21b, the applied pulling force along with the regulated grip force is shown for *taking* action with $\varphi = 20°$ and $\varphi = -20°$ respectively. The corresponding object accelerations can be found in Figures 21c and 21d. In both cases, the object is released immediately; note that in the case of $\varphi = -20°$, the object has negative downard acceleration after being released because it is pulled upward.

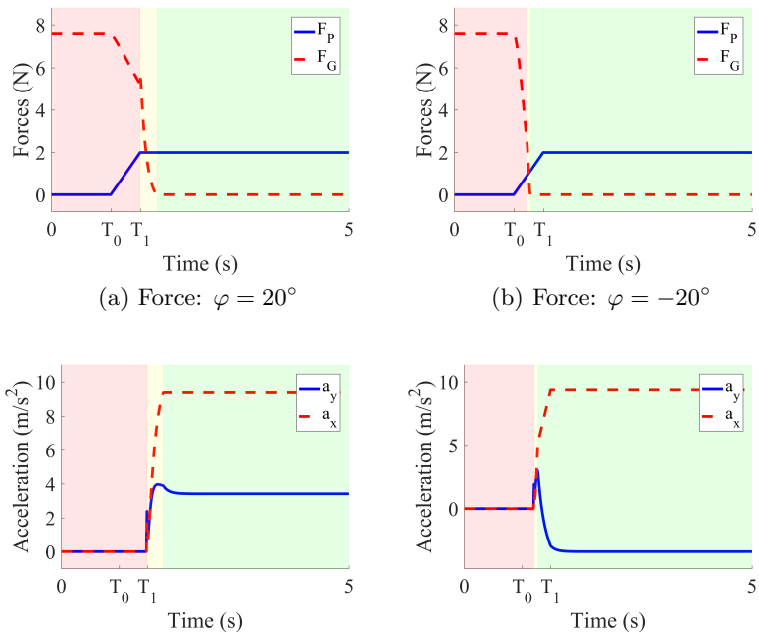

(a) Force: $\varphi = 20°$ (b) Force: $\varphi = -20°$

(c) Acceleration: $\varphi = 20°$ (d) Acceleration: $\varphi = -20°$

Figure 21. Applied pulling force and grip force in *taking* with (a) $\varphi = 20°$ and (b) $\varphi = -20°$. Acceleration of the object in *taking* with (c) $\varphi = 20°$ and (d) $\varphi = -20°$. Red background indicates the *grasp mode*, yellow the *slipping mode* and green the *release mode*.

In order to investigate the effect of the friction coefficient on the behavior of the system, the simulation is repeated with $\varphi = 0°$, this time with two different friction coefficients. In Figures 22a and 22b, the object acceleration is shown for the *taking* and the *dropping* actions for a surface with high friction ($\mu_s = 0.9, \mu_k = 0.8$). In Figures 22c and 22d, the object acceleration is shown for the same actions for a surface with low friction ($\mu_s = 0.3, \mu_k = 0.2$). In both of the *taking* cases, the object is released immediately after being pulled as expected. In the *dropping* cases, the object is not released and the grasp is re-established after the pulling

force is removed, although the object's slipping acceleration is higher in the system with low friction.

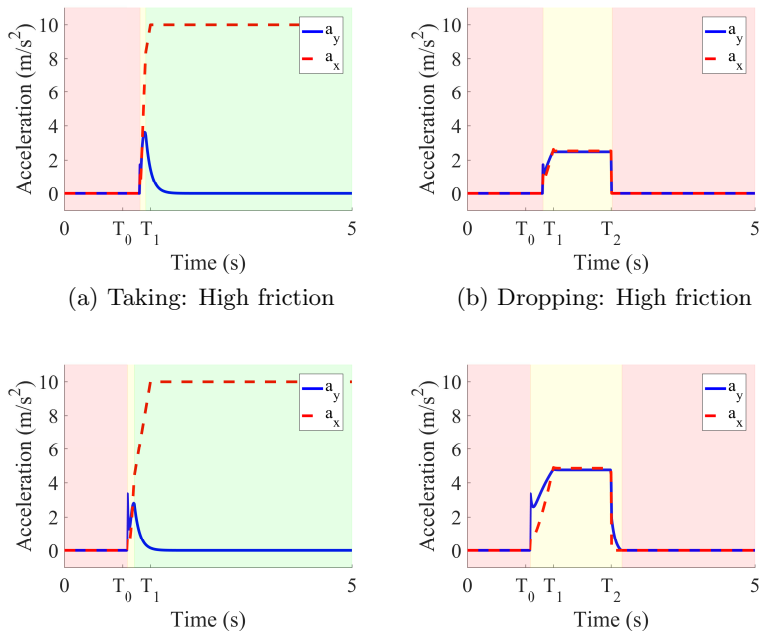

(a) Taking: High friction

(b) Dropping: High friction

(c) Taking: Low friction

(d) Dropping: Low friction

Figure 22. Acceleration of the object in (a) *taking* with high friction, (b) *dropping* with high friction, (c) *taking* with low friction and (d) *dropping* with low friction grippers. Red background indicates the *grasp mode*, yellow the *slipping mode* and green the *release mode*.

The next simulation investigates the sensitivity of the system. In Figures 23a and 23c, the forces applied to the object and the object's acceleration are shown for the *dropping* action under the presence of a white Gaussian noise ($SNR = 3dB$) applied to F_G. It can be seen

that the object's downward acceleration is still maintained below $6m/s^2$ and the grasp is re-established after the pulling is stopped. In Figures 23b and 23d, the same signals are shown in a *dropping* action while there is a white Gaussian noise ($SNR = 3dB$) applied to a_y. The figure clearly shows that the system is able to prevent the object from falling and re-establishes the grasp after the pulling is stopped. This shows that the overall performance of the system is quite robust against the sensor noise and the gripper disturbance.

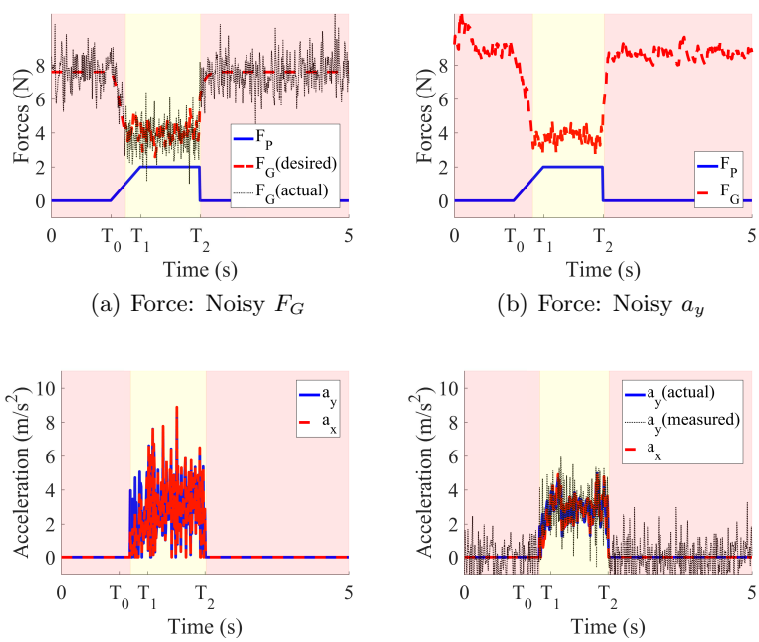

(a) Force: Noisy F_G (b) Force: Noisy a_y

(c) Acceleration: Noisy F_G (d) Acceleration: Noisy a_y

Figure 23. Applied pulling force and grip force in *dropping* with (a) disturbance applied to F_G and (b) noise applied to a_y. Acceleration of the object in *dropping* with (c) disturbance appied to F_G and (b) noise applied to a_y. Red background indicates the *grasp mode*, yellow the *slipping mode* and green the *release mode*.

3.6 Implementation and Experiments

Our proposed fail-safe (FS) handover controller is implemented on a Baxter robot [45] with a parallel gripper [70] installed on one of the robot's arms. In order to control the grip force, we used an open-loop position-based method: a small metal plane is added to one of the fingers of the gripper with a linear spring between the plane and the finger. Therefore, the grip force can be controlled based on the gripper position:

$$F_G(x) = \begin{cases} k(x - x_0), & x > x_0 \\ 0, & x \leq x_0 \end{cases} \tag{3.21}$$

where k is the stiffness of the spring, x is the gripper position command and x_0 is the position at which the gripper touches the object. The stiffness of the spring (k) was experimentally determined to be $5(N/cm)$. The gripper position control loop operates at 25Hz.

In order to measure the applied force, a SI-65-5 ATI Gamma force sensor [46] is added to the robot's arm between the end effector and the gripper. The force sensor output is sampled at 100Hz and the data is transferred to a computer through a PCI-6034 NI data acquisition board [47]. A 6cm×7cm×17cm empty box is used as the test object. The object weight is 230±5 mg. The object downward acceleration is measured through an ADNS-2051 optical sensor [62] installed on one of the fingers of the gripper. The object, the gripper and the installed devices on the gripper are shown in Figure 24.

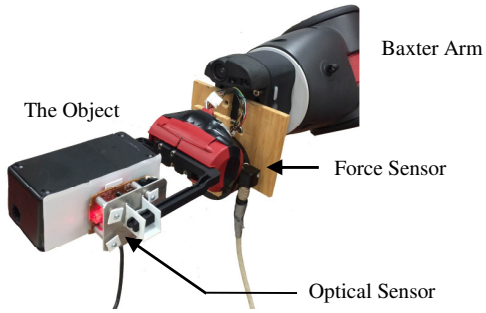

Figure 24. The experimental setup.

3.6.1 Experiment One: Evaluating the smoothness of the controller

In order to evaluate the smoothness of our FS controller and to fine-tune the parameters of the controller, we designed a robot-to-human handover experiment. Baxter would hand the object over to human subjects, using different controllers. In each trial, Baxter grasps the object within its electrical gripper. The handover controller is then activated and a beep sound is played for the subject. Participants are told to take the object from the robot, after hearing the beep sound.

3.6.1.1 Handover Controllers

We began with implementing the Fail-safe handover controller with the same parameters used in the simulations (see Table IV). Prior to experiment one, we conducted a pilot study with four participants (in addition to the subjects in experiment one), to see if the controller can perform the handover task smoothly without dropping the object. We realized that the system is very sensitive to measured force noise and in several cases, it dropped the object

before the participants touched it. Therefore, we decided to increase the force overshoot by decreasing parameter γ, from 5 to 3. Also we increased F_{margin} from 12N to 15N to increase the maximum tolerated object's downward acceleration.

We used four different handover controllers in experiment one: (a) first Fail-safe handover controller (FS1) with parameters $\alpha = 10, \beta = 3, \gamma = 3, F_{margin} = 15$. $k_i = 0.13$. This controller should have a performance similar to the controller used in the simulations. According to Figure 18, with having $\gamma = 3$, the force overshoot is about 2N when pulling forward ($F_{ST}(\varphi = 0) \simeq 2N$); (b) second Fail-safe handover controller (FS2) with parameters similar to FS1, except that α was increased to 15. This controller is used in the experiment to investigate the effect of changing parameter α. According to Equation 3.12, this controller has force overshoot about 4N when pulling forward; (c) third Fail-safe handover controller (FS3) with parameters similar to the FS1 controller, except that γ was decreased to 1. this controller is used in the experiment to investigate the effect of changing parameter γ. The force overshoot is about 3N when pulling forward; (d) the forth controller is Human-Inspired handover controller (HI) [3].

The human inspired handover controller was proposed in [3] and it was shown to have a smooth performance compared to the other existing handover controllers. We thus wanted to compare the smoothness of our FS controller to that of the HI controller. The HI controller regulates the grip force according to the object's load force, in a linear fashion:

$$F_G(F_L) = mF_L + F_{ZLG} \tag{3.22}$$

where F_G is the applied grip force, F_L is the object's gravitational load force acting on the robot's gripper, m is a constant slope and F_{ZLG} is a non-zero amount of grip force applied at zero load force that acts as a safety margin [3].

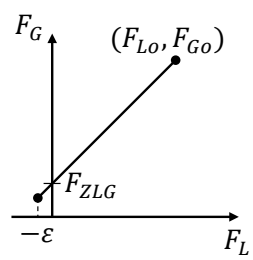

Figure 25. Grip force produced by the human inspired (HI) handover controller [3].

The HI controller output is illustrated in Figure 25. In the figure, F_{Lo} is the total weight of the object supported by the robot at the begining of the handover when the robot has stably grasped the object. At this time, the robot applies an initial grip force of F_{Go} that has been properly calculated so the object does not slip. A slight upward pulling force of ε has to be applied to the object, so it is completely released. The slope parameter (m) can be calculated based on F_{Lo}, F_{Go} and F_{ZLG}. We selected the controller parameters so that it mimics the behavior of *Controller A* introduced in [3], which was shown to be preferred by humans: F_{Go} was set to $15N$ to have an initial stable grasp, ε was set to $-2N$ (according to the results of

the human-human study in [2] for *Controller A*), and F_{ZLG} was set to $5N$ to account for the sensor measurement errors.

3.6.1.2 Experimental Procedure

Each participant compares three pairs of controllers: (FS1 vs. FS2), (FS1 vs. FS3) and (FS1 vs. HI). In each comparison, the robot hands over the object two times with one controller, followed by another two times using the other controller. After a set of four trials, the subject is asked to answer a survey evaluating the behavior of the robot in the first two trials compared to the second two trials. To eliminate ordering effects, each controller pair was presented to the participants in both orders. That results in a total of 6 pairwise comparisons and 24 trials. To balance the carryover effects, we used a complete Latin square design [71].

To observe the effect of the pulling direction on the results, the participants are asked to perform the entire procedure twice, once while standing and once while sitting, resulting in a total of 48 trials per participant. We expected that the participants would pull the object in different direction when they are sitting compared to standing situation.

We put a table with dimension ($L : 75cm$;$W : 60cm$;$H : 70cm$) at a distance of $70cm$ in front of the robot. The subject is sitting/standing across the table at a distance of $15cm$ from the edge of the table. The object is transferred at a height=$25cm$ above the table and at a distance=$40cm$ from the edge of the table in front of the subject. Figure 26 shows the position of the subject and the robot in standing and sitting cases.

The survey questions are:

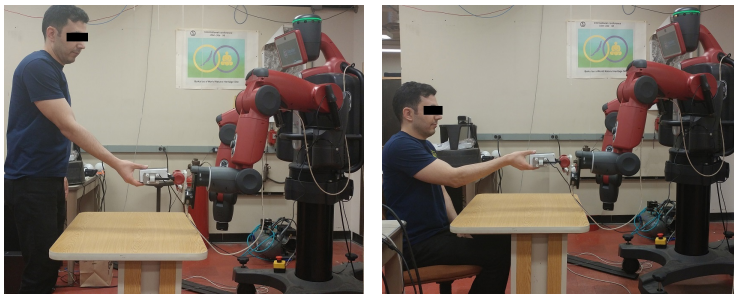

(a) (b)

Figure 26. Robot to human handover experiment: (a) standing case; (b) sitting case.

1. Rate how easy it was to take the object from the robot in the first two trials. There are five options, *very easy*, *easy*, *moderate*, *hard* and *very hard*.
2. Rate how easy it was to take the object from the robot in the second two trials. There are five options, *very easy*, *easy*, *moderate*, *hard* and *very hard*.
3. Do you prefer the robot behavior in the first two trials or in the second two trials? There are three options, *I prefer the robot behavior in the first two trials*, *I prefer the robot behavior in the second two trials*, and *No preference*.

For the study, 18 participants (13 males and 5 females) between ages 21 to 39 were recruited from students and staff at the University of Illinois at Chicago (UIC), by posting flyers and sending emails to UIC graduate students email-list. Before starting the experiment and to get familiar with the robot, each participant performed the handover task 8 times while standing, including 2 times with each controller in a random order. Participants were informed that there

is no movement in the robot's arm during the task. No further instructions were provided to the participants about how to take the object.

3.6.1.3 Results

We used the sign test [61] to analyze the survey responses.

3.6.1.3.1 Standing case

Significantly more participants responded that they prefer the FS1 controller over HI controller (Z=-3.031,p=0.0024) and also over FS2 controller (Z=-3.241,p=0.0012).

Participants' ratings for how easy it was to take the object from the robot did not significantly differ between the FS1 controller and the HI controller (Z=-1.18,p=0.238), or between the FS1 controller and FS3 controller (Z=-1.34,p=0.180). However, significantly more participants responded that the object can be more easily taken from the robot with the FS1 controller compared to the FS2 controller (Z=-2.932,p=0.0034).

While the system is in the *grasp mode*, the applied pulling force can be calculated using Equation 3.3 and Equation 3.5. The average applied pulling force and the average produced grip force for the standing trials are shown in Figure 27 for all of the controllers. The force signals are normalized over time ($t = 1$ shows the time that the object is released). Force overshoot for each controller can be determined from Figure 27a by measuring the maximum pulling force applied before the object is released. It can be seen in Figure 27a that the FS1 controller force overshoot ($\sim$2N) is smaller compared to other controllers.

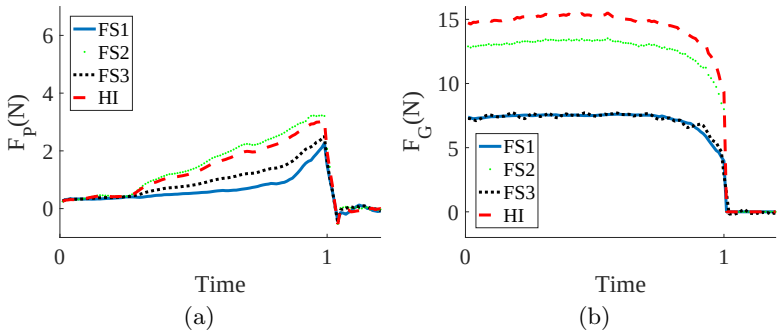

Figure 27. (a) Average applied pulling force, (b) average grip force for all of the controllers - standing trials. Force signals are normalized over time.

3.6.1.3.2 Sitting case

We speculated that in the sitting case, a subject would pull the object almost horizontally as the object is in front of his/her upper body. Since the HI controller can only handle vertical object transfer, we predicted the force overshoot for this controller to be significantly higher when the user tries to take the object horizontally. We also predicted larger force overshoot for the FS2 and FS3 controllers in this case, since $F_{ST}(\varphi = 0)$ is larger for these controllers compared to the FS1 controller. The average applied pulling force and the average produced grip force for sitting trials are shown in Figure 28 for all of the controllers. The force signals are normalized over time ($t = 1$ shows the time when the object is released). It can be seen in Figure 28a that the FS1 controller force overshoot ($\sim$2N) is smaller compared to other controllers. In fact in this case, there is a significant difference between the force overshoot of the FS1 controller and that of the other controllers.

The survey analysis shows that in the sitting case, significantly more participants responded that the object can be more easily taken from the robot with the FS1 controller compared to the HI controller (Z=-3.171,p<0.0016), to the FS2 controller (Z=-3.171,p<0.0016), and also to the FS3 controller (Z=-2.428,p<0.016). Also, significantly more participants responded that they prefer the FS1 controller over the HI controller (Z=-3.53,p<0.0005), over FS2 controller (Z=-3.591,p<0.0004), and also over FS3 controller (Z=-3.103,p=0.0019). The subject preference ratings can be explained by the smaller force overshoot of FS1 controller.

In summary, we conclude that the FS1 controller shows a superior performance compared to the other controllers in terms of the force overshoot (smoothness) and the subject preference ratings.

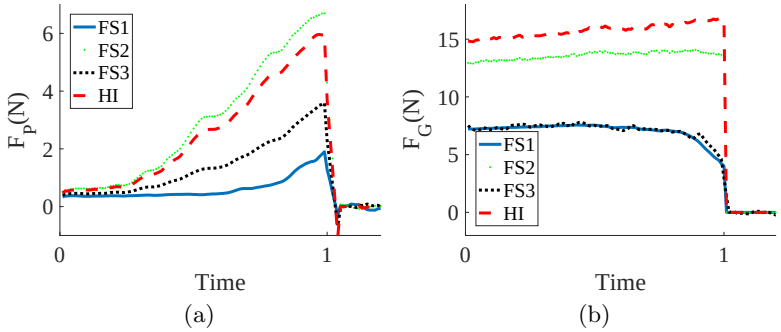

Figure 28. (a) Average applied pulling force, (b) average grip force for all of the controllers - sitting trials. Force signals are normalized over time.

3.6.2 Experiment Two: Evaluating the object safety

The second experiment is designed to evaluate the object safety. Following the same method that we used in Section 3.5, a failure is simulated for the robot: a forward pulling force of specified magnitude is applied to the object without compensating the weight of the object. A rope is attached to the object with an analog force meter attached to the rope. At $t = 3s$ the rope is pulled with $F_p = 2N$ and $\varphi = 0$. For this experiment we use FS1 controller from Section 3.6.1 which showed superior performance compared to the other controllers.

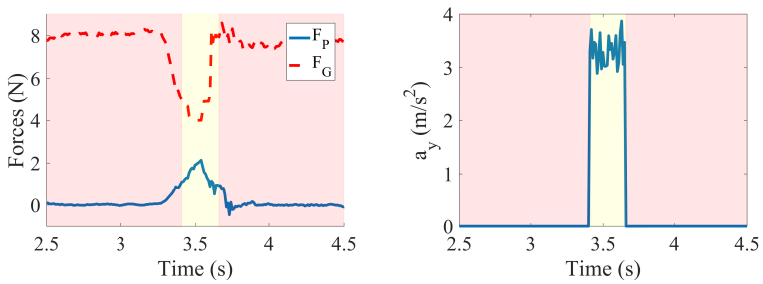

(a) Force (b) Acceleration

Figure 29. Problematic handover: (a) applied pulling force and the grip force; (b) the object downward acceleration a_y.

Figure 29 shows the applied pulling force, the generated grip force and the object downward acceleration. As it is shown in Figure 29b, the object downward acceleration a_y is kept below $4m/s^2$ while the pulling force is applied. That means that the object is not released completely

and the system has remained in the *slipping mode*, successfully preventing the object from falling.

3.7 Discussion

In this chapter, we proposed a novel framework for ensuring a safe and smooth robot-to-human handover. The framework critically depends on the ability of the robot to readily detect a failure during the handover and effectively recover from it. This in turn motivated us to study how humans detect failure when they play the role of a giver. Towards this goal, we conducted a human study to investigate which sensing modality is used by humans to detect failure. In particular, we examined whether haptic sensing plays the dominant role in detecting failure, or the human givers primarily depend on vision. The results suggest that at least in some scenarios, haptic sensing is not reliable enough to determine whether the object is dropped or successfully taken by the receiver after being released, and that humans seem to rely on vision. Motivated by this finding we proposed a robot handover architecture that relies on measuring relative motion between the object and the robot hand, provided through an optical sensor, to detect an impending handover failure. In turn, a handover controller was proposed that uses the measurement of object acceleration in the feedback loop to guarantee handover safety. At the same time, by monitoring the force applied on the object, the controller achieves smoothness of the handover. The proposed architecture thus overcomes the shortcomings of the existing controllers that trade off smoothness for safety, or vice versa.

We provided a detailed analysis of the proposed controller. The controller is designed to work in three different modes: *grasping*, *slipping* and the *release mode*. One of our main con-

ceptual contributions is to explicitly model the *slipping mode*. The *slipping mode* characterizes the transfer phase of the handover and is therefore critical for both safety and smoothness. By monitoring the object acceleration and applied forces, the controller is able to distinguish between a slipping object that is falling and a slipping object that is being transferred from the robot's hand to the human. Performance of the proposed handover controller was first investigated through simulation and it was shown that the controller is quite robust. Also, we showed experimentally and by assessing human satisfaction that the proposed system demonstrates significantly higher performance compared to other handover controllers. Given that the proposed system is inexpensive and easy to implement on general robot hardware, we believe that it represents a significant step towards improving physical human-robot interaction.

CHAPTER 4

CONCLUSIONS AND FUTURE WORK

4.1 A Comprehensive Robot-to-Human Handover System

In this work, we studied the reaching out phase and the transfer phase of an object handover. These are the two phases in which there is physical interaction between the actors. In Chapter 2, we studied the reaching motion of a human giver in human-human handovers and proposed a dyadic joint torque (DTJ) model that can estimate the object transfer position, based on kinematics and body weight of the human actors. Besides that, we investigated the velocity of the giver's reaching motion and showed that unless there is a physical constraint, the velocity is independent of the task conditions including the object type and the actors' pose. We evaluated the DJT model in a robot-to-human handover experiment and showed that the model will generate object transfer position at desired height above the ground and comfortable distance from the human.

In Chapter 3, we proposed a novel handover system that consists of an acceleration sensor mounted on the robot gripper and a fail-safe controller. Our fail-safe controller has the ability to recover from a handover failure by re-grasping the object. We showed experimentally that the proposed system exhibits significantly higher performance compared to other handover controllers in terms of smoothness and safety of the task. Our other contribution is that we proposed a setup in which all the required sensors are embedded in the robot's hand. This makes

our system more practical for use in everyday applications. Also, it is possible to implement the proposed system on any robot which possesses a simple two finger gripper.

The final goal in this research is to develop a comprehensive handover system implemented in ROS which manages to perform all the steps of a robot to human handover task autonomously. We use Baxter Robot for the implementation of the proposed system. The software architecture of the system is shown in Figure 30.

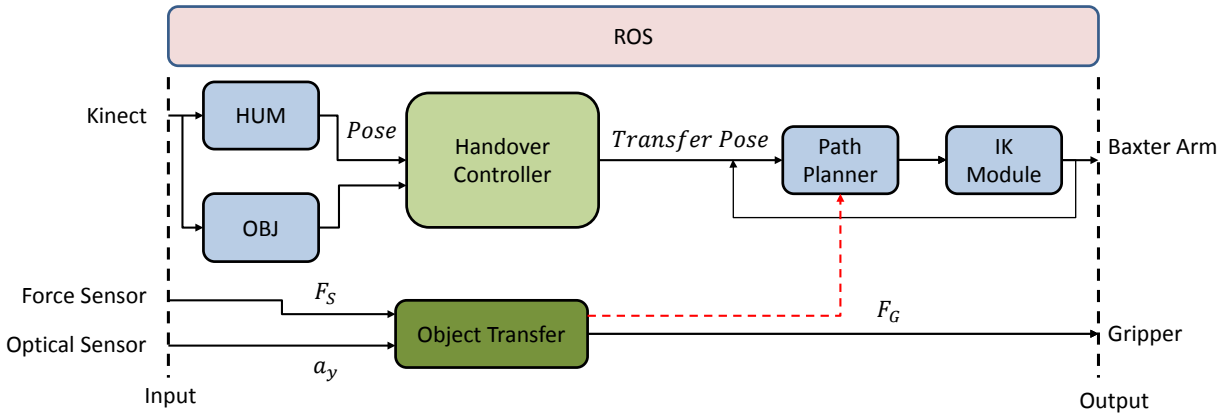

Figure 30. The comprehensive handover system.

The system consists of two main controllers (the green blocks in Figure 30). `Object Transfer`, working at 10Hz, is responsible for the object transfer phase. It receives the applied force to the object (F_S) and the object downward acceleration (a_y) and regulates the grip

force (F_G) applied by the gripper. A block diagram of this controller is presented in Figure 17 (the controller is discussed in Section 3.4.2).

`Handover Controller`, working at 100Hz, is responsible for the grasp and the reaching out phases. First, the initial position of the object is obtained from `OBJ`. `Handover Controller` sends the command to the path planner, so the robot moves its arm to pickup the object. After grasping the object, `Handover Controller` calculates the object transfer position ($TransferPose$) based on the human pose and his/her kinematics, using our DJT model proposed in Section 2.4.1. The human pose and kinematics are obtained from `HUM` block. $TransferPose$ is sent as a command to the path planner. `Path Planner` plans and implements a linear minimum jerk trajectory to the commanded position. It uses the inverse kinematics of the robot (`IK Module`) to compute the required joint values at each iteration.

The two controllers work almost independently, except the *release interrupt* path (showed by a dashed red line in Figure 30). Whenever the object is fully released by the robot, the `Object Transfer` sends an interrupt signal to the `Path Planner` and stops any further movement.

`HUM` computes the pose and the kinematics of the human, and `OBJ` estimates the initial position of the object. These blocks receive input from a Kinect sensor. Microsoft developed Kinect, as a motion tracking sensor mainly for Xbox video game consoles. Images from Kinect provide raw depth and RGB color at 30Hz. Several software packages have been developed that extract human tracking data by processing the images from Kinect. OpenNI is one of the tools that provides a 14-point skeleton outlining the human's pose (see Figure 31).

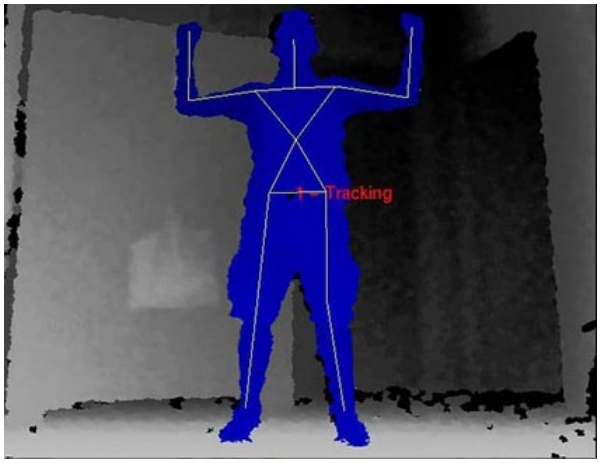

Figure 31. Human tracking with OpenNI.

Although the Kinect human tracking system is reliable, there are several issues with the tracked position of the hand. These errors occur when the human is moving fast or when there are other objects near the human. Mincelli *et al.* [72], proposed two corrections in order to improve the tracking system performance. In case the Kinect output lags the true human motion, the hand position is moved to the closest 3D point in a small box around the estimated point by Kinect (see Figure 32a). It is reported that this correction has a fast response and it is robust against the noise in the estimated human pose.

During the final phase of a handover, the robot's hand gets close to the human's hand. At this point the robot partially merges into the human's point cloud. In the correction method proposed in [72], the information about the joint configuration of the robot is used to determine the position of the robot's hand and if it is closer than 15cm to the human's hand, the estimated

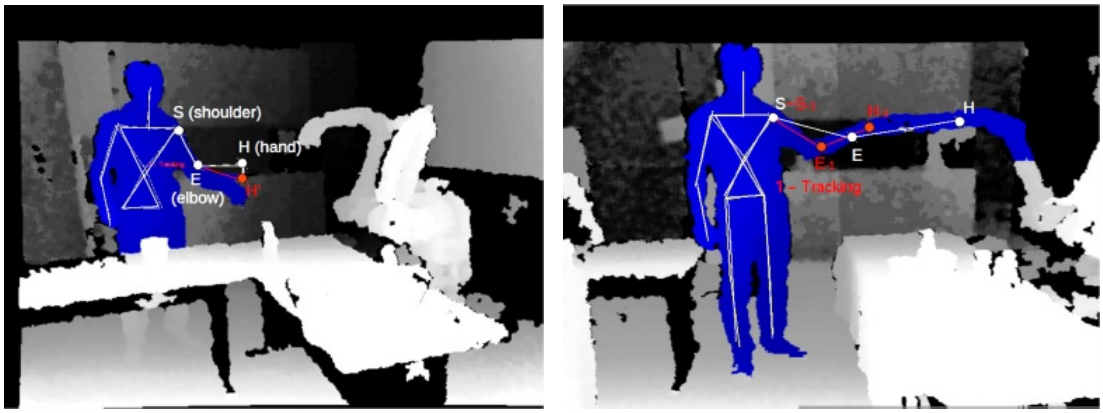

(a) (b)

Figure 32. Skeleton tracking correction. White lines: OpenNI skeleton tracker output. Red lines:corrected hand position. Figure from Mincelli *et al.*

position of the human's hand is filtered out (See Figure 32b). This approximation is based on the assumption that the human does not move much when very close to the robot.

While the performance of each controller in Figure 30 is evaluated through human-robot experiments in Chapters 2 and 3, due to the mentioned practical limitations of the human tracking sensor, we were unable to experimentally evaluate the performance of the whole system. With the current fast progress rate in the virtual reality (VR) technology, it is expected to have more reliable tracking sensors available to be used in the proposed handover system in near future.

4.2 Future Work

One possible extention of this work is to design a *human-to-robot* handover controller. In most of the previous studies that address human-to-robot handover, it is the human who has

to position and orient the object into the robot's hand and then push it, so the robot perceives that it should close its hand. However, there are only few works in which the robot actively takes the object instead of receiving it. The main reason is the challenge of reliably tracking the human's hand. By introducing human tracking systems like the Kinect sensor, researches began to develop handover systems in which the robot locates the human's hand, and then reaches out to take the object [24, 72]. Kinect sensor is also used for identifying if an object was held by the human, recognizing the object type and calculating where the robot should put its hand for the handover.

The final step in human-to-robot handover is to grasp the object by closing the gripper. In [72], two methods are proposed to trigger a gripper closing command: detecting a force applied to the robot's hand and a timeout. It is reported that sometimes users do not intuitively know that they have to push the object into the robot's hand, so the timeout trigger is added to the system. On the other hand, the timeout itself can make the robot seem aggressive to the user. The issue of triggering the gripper closing command is similar to the problem of releasing the object in a robot-to-human handover discussed in Section 3.1. We propose to add an optical sensor to the gripper both to measure the object acceleration and to detect the object presence. Based on the measured object acceleration, we can prevent the object from falling in case of an imperfect handover.

APPENDIX

COPYRIGHT PERMISSIONS

Here, we present the copyright permissions for the article [1] whose contents were used in Chapter 3, and article [23] whose contents were used in Chapter 2 of this thesis.

Title: A fail-safe object handover controller

Conference Proceedings: Robotics and Automation (ICRA), 2016 IEEE International Conference on

Author: Sina Parastegari

Publisher: IEEE

Date: May 2016

Thesis / Dissertation Reuse

The IEEE does not require individuals working on a thesis to obtain a formal reuse license, however, you may print out this statement to be used as a permission grant:

Requirements to be followed when using any portion (e.g., figure, graph, table, or textual material) of an IEEE copyrighted paper in a thesis:

1) In the case of textual material (e.g., using short quotes or referring to the work within these papers) users must give full credit to the original source (author, paper, publication) followed by the IEEE copyright line © 2011 IEEE.
2) In the case of illustrations or tabular material, we require that the copyright line © [Year of original publication] IEEE appear prominently with each reprinted figure and/or table.
3) If a substantial portion of the original paper is to be used, and if you are not the senior author, also obtain the senior author's approval.

Requirements to be followed when using an entire IEEE copyrighted paper in a thesis:

1) The following IEEE copyright/ credit notice should be placed prominently in the references: © [year of original publication] IEEE. Reprinted, with permission, from [author names, paper title, IEEE publication title, and month/year of publication]
2) Only the accepted version of an IEEE copyrighted paper can be used when posting the paper or your thesis on-line.
3) In placing the thesis on the author's university website, please display the following message in a prominent place on the website: In reference to IEEE copyrighted material which is used with permission in this thesis, the IEEE does not endorse any of [university/educational entity's name goes here]'s products or services. Internal or personal use of this material is permitted. If interested in reprinting/republishing IEEE copyrighted material for advertising or promotional purposes or for creating new collective works for resale or redistribution, please go to http://www.ieee.org/publications_standards/publications/rights/rights_link.html to learn how to obtain a License from RightsLink.

If applicable, University Microfilms and/or ProQuest Library, or the Archives of Canada may supply single copies of the dissertation.

Title: Modeling human reaching phase in human-human object handover with application in robot-human handover

Conference Proceedings: Intelligent Robots and Systems (IROS), 2017 IEEE/RSJ International Conference on

Author: Sina Parastegari

Publisher: IEEE

Date: Sept. 2017

Thesis / Dissertation Reuse

The IEEE does not require individuals working on a thesis to obtain a formal reuse license, however, you may print out this statement to be used as a permission grant:

Requirements to be followed when using any portion (e.g., figure, graph, table, or textual material) of an IEEE copyrighted paper in a thesis:

1) In the case of textual material (e.g., using short quotes or referring to the work within these papers) users must give full credit to the original source (author, paper, publication) followed by the IEEE copyright line © 2011 IEEE.
2) In the case of illustrations or tabular material, we require that the copyright line © [Year of original publication] IEEE appear prominently with each reprinted figure and/or table.
3) If a substantial portion of the original paper is to be used, and if you are not the senior author, also obtain the senior author's approval.

Requirements to be followed when using an entire IEEE copyrighted paper in a thesis:

1) The following IEEE copyright/ credit notice should be placed prominently in the references: © [year of original publication] IEEE. Reprinted, with permission, from [author names, paper title, IEEE publication title, and month/year of publication]
2) Only the accepted version of an IEEE copyrighted paper can be used when posting the paper or your thesis on-line.
3) In placing the thesis on the author's university website, please display the following message in a prominent place on the website: In reference to IEEE copyrighted material which is used with permission in this thesis, the IEEE does not endorse any of [university/educational entity's name goes here]'s products or services. Internal or personal use of this material is permitted. If interested in reprinting/republishing IEEE copyrighted material for advertising or promotional purposes or for creating new collective works for resale or redistribution, please go to http://www.ieee.org/publications_standards/publications/rights/rights_link.html to learn how to obtain a License from RightsLink.

If applicable, University Microfilms and/or ProQuest Library, or the Archives of Canada may supply single copies of the dissertation.

CITED LITERATURE

1. Parastegari, S., Noohi, E., Abbasi, B., and Zefran, M.: A Fail-safe Object Handover Controller. In Robotics and Automation (ICRA), 2016 IEEE International Conference on, 2016.

2. Chan, W. P., Parker, C. A. C., Loos, H. F. M. V. d., and Croft, E. A.: Grip forces and load forces in handovers: Implications for designing human-robot handover controllers. In 2012 7th ACM/IEEE International Conference on Human-Robot Interaction (HRI), pages 9–16, March 2012.

3. Chan, W. P., Parker, C. A., Van Der Loos, H. M., and Croft, E. A.: A human-inspired object handover controller. The International Journal of Robotics Research, 32(8):971–983, 2013.

4. Mason, A. H. and MacKenzie, C. L.: Grip forces when passing an object to a partner. Experimental brain research, 163(2):173–187, 2005.

5. Shibata, S., Tanaka, K., and Shimizu, A.: Experimental analysis of handing over. In Robot and Human Communication, 1995. RO-MAN'95 TOKYO, Proceedings., 4th IEEE International Workshop on, pages 53–58. IEEE, 1995.

6. Basili, P., Huber, M., Brandt, T., Hirche, S., and Glasauer, S.: Investigating human-human approach and hand-over. In Human Centered Robot Systems, pages 151–160. Springer, 2009.

7. Sisbot, E. A., Alami, R., Simon, T., Dautenhahn, K., Walters, M., and Woods, S.: Navigation in the presence of humans. In Humanoid Robots, 2005 5th IEEE-RAS International Conference on, pages 181–188. IEEE, 2005.

8. Sisbot, E. A. and Alami, R.: A human-aware manipulation planner. Robotics, IEEE Transactions on, 28(5):1045–1057, 2012.

9. Edsinger, A. and Kemp, C. C.: Human-robot interaction for cooperative manipulation: Handing objects to one another. In Robot and Human interactive Communication, 2007. RO-MAN 2007. The 16th IEEE International Symposium on, pages 1167–1172. IEEE, 2007.

10. Glasauer, S., Huber, M., Basili, P., Knoll, A., and Brandt, T.: Interacting in time and space: Investigating human-human and human-robot joint action. In RO-MAN, 2010 IEEE, pages 252–257. IEEE, 2010.

11. Kajikawa, S., Okino, T., Ohba, K., and Inooka, H.: Motion planning for hand-over between human and robot. In Intelligent Robots and Systems 95.'Human Robot Interaction and Cooperative Robots', Proceedings. 1995 IEEE/RSJ International Conference on, volume 1, pages 193–199. IEEE, 1995.

12. Hendrich, N., Bistry, H., Liebrecht, J., and Zhang, J.: Multi-modal clues for efficient human-robot object handover: a case study with elderly users. In Robot and Human Interactive Communication, 2014 RO-MAN: The 23rd IEEE International Symposium on. Workshop of New Frontiers of Service Robotics for the Elderly., 2014.

13. Nagata, K., Oosaki, Y., Kakikura, M., and Tsukune, H.: Delivery by hand between human and robot based on fingertip force-torque information. In Intelligent Robots and Systems, 1998. Proceedings., 1998 IEEE/RSJ International Conference on, volume 2, pages 750–757. IEEE, 1998.

14. Strabala, K. W., Lee, M. K., Dragan, A. D., Forlizzi, J. L., Srinivasa, S., Cakmak, M., and Micelli, V.: Towards seamless human-robot handovers. Journal of Human-Robot Interaction, 2(1):112–132, 2013.

15. Kim, J., Park, J., Hwang, Y. K., and Lee, M.: Advanced grasp planning for handover operation between human and robot. In 2nd International Conference on Autonomous Robots and Agents, pages 13–15, 2004.

16. Lopez-Damian, E., Sidobre, D., DeLaTour, S., and Alami, R.: Grasp planning for interactive object manipulation. In Proc. of the Intl. Symp. on Robotics and Automation, 2006.

17. Sadigh, M. J. and Ahmadi, H.: Safe grasping with multi-link fingers based on force sensing. In Robotics and Biomimetics (ROBIO), 2009 IEEE International Conference on, pages 1796–1802. IEEE, 2009.

18. Satake, S., Kanda, T., Glas, D. F., Imai, M., Ishiguro, H., and Hagita, N.: How to approach humans?-strategies for social robots to initiate interaction. In 2009 4th ACM/IEEE International Conference on Human-Robot Interaction (HRI), pages 109–116, March 2009.

19. Mumm, J. and Mutlu, B.: Human-robot proxemics: physical and psychological distancing in human-robot interaction. In Proceedings of the 6th international conference on Human-robot interaction, pages 331–338. ACM, 2011.

20. Strabala, K. W., Lee, M. K., Dragan, A. D., Forlizzi, J. L., Srinivasa, S., Cakmak, M., and Micelli, V.: Towards seamless human-robot handovers. Journal of Human-Robot Interaction, 2(1):112–132, 2013.

21. Cakmak, M., Srinivasa, S. S., Lee, M. K., Forlizzi, J., and Kiesler, S.: Human preferences for robot-human hand-over configurations. In Intelligent Robots and Systems (IROS), 2011 IEEE/RSJ International Conference on, pages 1986–1993. IEEE, 2011.

22. Srinivasa, S. S., Ferguson, D., Helfrich, C. J., Berenson, D., Collet, A., Diankov, R., Gallagher, G., Hollinger, G., Kuffner, J., and Weghe, M. V.: Herb: a home exploring robotic butler. Autonomous Robots, 28(1):5–20, 2010.

23. Parastegari, S., Abbasi, B., Noohi, E., and Zefran, M.: Modeling human reaching phase in human-human object handover with application in robot-human handover. In Intelligent Robots and Systems (IROS), 2017 IEEE/RSJ International Conference on, 2017.

24. Prada, M., Remazeilles, A., Koene, A., and Endo, S.: Implementation and experimental validation of Dynamic Movement Primitives for object handover. In Intelligent Robots and Systems (IROS 2014), 2014 IEEE/RSJ International Conference on, pages 2146–2153. IEEE, 2014.

25. Ijspeert, A. J., Nakanishi, J., Shibata, T., and Schaal, S.: Nonlinear dynamical systems for imitation with humanoid robots. In Proceedings of the IEEE/RAS International Conference on Humanoids Robots (Humanoids2001), pages 219–226, 2001.

26. Becchio, C., Sartori, L., and Castiello, U.: Toward you the social side of actions. Current Directions in Psychological Science, 19(3):183–188, 2010.

27. Agah, A. and Tanie, K.: Human interaction with a service robot: Mobile-manipulator handing over an object to a human. In Robotics and Automation, 1997. Proceedings., 1997 IEEE International Conference on, volume 1, pages 575–580. IEEE, 1997.

28. Koay, K. L., Sisbot, E. A., Syrdal, D. S., Walters, M. L., Dautenhahn, K., and Alami, R.: Exploratory Study of a Robot Approaching a Person in the Context of Handing

Over an Object. In AAAI spring symposium: multidisciplinary collaboration for socially assistive robotics, pages 18–24, 2007.

29. Huber, M., Rickert, M., Knoll, A., Brandt, T., and Glasauer, S.: Human-robot interaction in handing-over tasks. In Robot and Human Interactive Communication, 2008. RO-MAN 2008. The 17th IEEE International Symposium on, pages 107–112. IEEE, 2008.

30. Kajikawa, S. and Ishikawa, E.: Trajectory planning for hand-over between human and robot. In Robot and Human Interactive Communication, 2000. RO-MAN 2000. Proceedings. 9th IEEE International Workshop on, pages 281–287. IEEE, 2000.

31. Mainprice, J., Gharbi, M., Simon, T., and Alami, R.: Sharing effort in planning human-robot handover tasks. In RO-MAN, 2012 IEEE, pages 764–770. IEEE, 2012.

32. Pandey, A. K., Ali, M., Warnier, M., and Alami, R.: Towards multi-state visuo-spatial reasoning based proactive human-robot interaction. In Advanced Robotics (ICAR), 2011 15th International Conference on, pages 143–149. IEEE, 2011.

33. Aleotti, J., Micelli, V., and Caselli, S.: Comfortable robot to human object hand-over. In RO-MAN, 2012 IEEE, pages 771–776. IEEE, 2012.

34. Aleotti, J., Micelli, V., and Caselli, S.: An affordance sensitive system for robot to human object handover. International Journal of Social Robotics, 6(4):653–666, 2014.

35. Katayama, M. and Hasuura, H.: Optimization principle determines human arm postures and comfort. In SICE Annual Conference Program and Abstracts SICE Annual Conference 2003, pages 47–47. The Society of Instrument and Control Engineers, 2003.

36. Van Bolhuis, B. and Gielen, C.: A comparison of models explaining muscle activation patterns for isometric contractions. Biological cybernetics, 81(3):249–261, 1999.

37. Bolhuis, B. v., Gielen, C., and Ingen Schenau, G. v.: Activation patterns of mono-and bi-articular arm muscles as a function of force and movement direction of the wrist in humans. The Journal of physiology, 508(1):313–324, 1998.

38. Cholewicki, J., McGill, S. M., and Norman, R. W.: Comparison of muscle forces and joint load from an optimization and emg assisted lumbar spine model: towards development of a hybrid approach. Journal of biomechanics, 28(3):321–331, 1995.

39. Collins, J.: The redundant nature of locomotor optimization laws. Journal of biomechanics, 28(3):251–267, 1995.

40. Bogin, B. and Varela-Silva, M. I.: Leg length, body proportion, and health: a review with a note on beauty. International journal of environmental research and public health, 7(3):1047–1075, 2010.

41. Abdel-Aziz, Y. and Karara, H.: Direct linear transformation into object space coordinates in close-range photogrammetry, in proc. symp. close-range photogrammetry. Urbana-Champaign, pages 1–18, 1971.

42. Mauchly, J. W.: Significance test for sphericity of a normal n-variate distribution. The Annals of Mathematical Statistics, 11(2):204–209, 1940.

43. Greenhouse, S. W. and Geisser, S.: On methods in the analysis of profile data. Psychometrika, 24(2):95–112, 1959.

44. Dunn, O. J.: Multiple comparisons among means. Journal of the American Statistical Association, 56(293):52–64, 1961.

45. Rethink Robotics Baxter. `http://www.rethinkrobotics.com/baxter/`, 2016.

46. ATI Industrial Automation, F/T Sensor. `http://www.ati-ia.com/products/ft/ft_models.aspx?id=Gamma`, 2016.

47. National Instruments, NI PCI-6034E (Legacy),. `http://sine.ni.com/nips/cds/view/p/lang/en/nid/11916`.

48. Johansson, R. S. and Westling, G.: Roles of glabrous skin receptors and sensorimotor memory in automatic control of precision grip when lifting rougher or more slippery objects. Experimental brain research, 56(3):550–564, 1984.

49. Deyle, T., Nguyen, H., Reynolds, M., and Kemp, C.: Rfid-guided robots for pervasive automation. IEEE Pervasive Computing, 9(2):37–45, 2010.

50. Bohren, J., Rusu, R. B., Jones, E. G., Marder-Eppstein, E., Pantofaru, C., Wise, M., Msenlechner, L., Meeussen, W., and Holzer, S.: Towards autonomous robotic butlers: Lessons learned with the PR2. In Robotics and Automation (ICRA), 2011 IEEE International Conference on, pages 5568–5575. IEEE, 2011.

51. Tremblay, M. R. and Cutkosky, M. R.: Estimating friction using incipient slip sensing during a manipulation task. In Robotics and Automation, 1993. Proceedings., 1993 IEEE International Conference on, pages 429–434. IEEE, 1993.

52. Roberts, L., Singhal, G., and Kaliki, R.: Slip detection and grip adjustment using optical tracking in prosthetic hands. In Engineering in Medicine and Biology Society, EMBC, 2011 Annual International Conference of the IEEE, pages 2929–2932. IEEE, 2011.

53. Canepa, G., Petrigliano, R., Campanella, M., and De Rossi, D.: Detection of incipient object slippage by skin-like sensing and neural network processing. Systems, Man, and Cybernetics, Part B: Cybernetics, IEEE Transactions on, 28(3):348–356, 1998.

54. Melchiorri, C.: Slip detection and control using tactile and force sensors. Mechatronics, IEEE/ASME Transactions on, 5(3):235–243, 2000.

55. Johansson, R. S. and Westling, G.: Tactile afferent signals in the control of precision grip. In Attention and Performance, volume 13, pages 677–713. Lawrence Erlbaum Associates, Inc, 1990.

56. Cipriani, C., Zaccone, F., Micera, S., and Carrozza, M. C.: On the shared control of an EMG-controlled prosthetic hand: analysis of userprosthesis interaction. Robotics, IEEE Transactions on, 24(1):170–184, 2008.

57. Yussof, H., Wada, J., and Ohka, M.: Analysis of tactile slippage control algorithm for robotic hand performing grasp-move-twist motions. Int. J. Smart Sens. Intell. Syst, 3(3):359–375, 2010.

58. Ajoudani, A., Hocaoglu, E., Altobelli, A., Rossi, M., Battaglia, E., Tsagarakis, N., and Bicchi, A.: Reflex control of the pisa/iit softhand during object slippage. In Robotics and Automation (ICRA), 2016 IEEE International Conference on, pages 1972–1979. IEEE, 2016.

59. SparkFun 9 Degrees of Freedom - Sensor Stick - SEN-10724 - SparkFun Electronics. `https://www.sparkfun.com/products/10724`.

60. Arduino - ArduinoBoardMega. `https://www.arduino.cc/en/Main/arduinoBoardMega`.

61. Wackerly, D., Mendenhall, W., and Scheaffer, R.: Mathematical statistics with applications. Nelson Education, 2007.

62. ADNS2051 Datasheet(PDF) - Agilent(Hewlett-Packard). http://www.alldatasheet.com/datasheet-pdf/pdf/102949/HP/ADNS2051.html.

63. Buerger, S. P. and Hogan, N.: Complementary stability and loop shaping for improved humanrobot interaction. Robotics, IEEE Transactions on, 23(2):232–244, 2007.

64. Miller, B. E., Colgate, J. E., and Freeman, R. A.: Guaranteed stability of haptic systems with nonlinear virtual environments. Robotics and Automation, IEEE Transactions on, 16(6):712–719, 2000.

65. Kazerooni, H.: Human-robot interaction via the transfer of power and information signals. Systems, Man and Cybernetics, IEEE Transactions on, 20(2):450–463, 1990.

66. Duchaine, V. and Gosselin, C. M.: Investigation of human-robot interaction stability using Lyapunov theory. In Robotics and Automation, 2008. ICRA 2008. IEEE International Conference on, pages 2189–2194. IEEE, 2008.

67. Colgate, J. E. and Schenkel, G. G.: Passivity of a class of sampled-data systems: Application to haptic interfaces. Journal of robotic systems, 14(1):37–47, 1997.

68. Tsumugiwa, T., Yokogawa, R., and Yoshida, K.: Stability analysis for impedance control of robot for human-robot cooperative task system. In Intelligent Robots and Systems, 2004.(IROS 2004). Proceedings. 2004 IEEE/RSJ International Conference on, volume 4, pages 3883–3888. IEEE, 2004.

69. Adams, R. J. and Hannaford, B.: Stable haptic interaction with virtual environments. Robotics and Automation, IEEE Transactions on, 15(3):465–474, 1999.

70. Accessories to Customize Your Baxter. http://www.rethinkrobotics.com/accessories/.

71. van Lint, J. H. and Wilson, R. M.: A course in combinatorics. Cambridge university press, 2001.

72. Micelli, V., Strabala, K., and Srinivasa, S.: Perception and control challenges for effective human-robot handoffs. 2011.

VITA

Sina Parastegari

Education

- Ph.D. Electrical and Computer Engineering, University of Illinois at Chicago 2013-2017
  Dissertation: Modelling and Control of Object Handover, A study in Human-Robot Interaction
- M.Sc. Electrical and Computer Engineering, University of Tehran 2009-2012
  Thesis: Intelligent Control of Wheel-tip Robot Manipulator
- B.Sc. Electrical and Computer Engineering, Isfahan University of Technology 2005-2009

Publications

- S. Parastegari, B. Abbasi, E. Noohi and M. Ẑefran, "Modeling Human Reaching Phase in Human-Human Object Handover with Application in Robot-Human Handover." Intelligent Robots and Systems (IROS 2017), 2017 IEEE/RSJ International Conference on. IEEE, 2017.
- S. Parastegari, E. Noohi, B. Abbasi and M. Ẑefran, "Failure Recovery in Robot-Human Object Handover." IEEE Transactions on Robotics, accepted for publication, Sep. 2017.
- S. Parastegari, E. Noohi, B. Abbasi and M. Ẑefran, "A fail-safe object handover controller." Robotics and Automation (ICRA), 2016 IEEE International Conference on. IEEE, 2016.
- B. Abbasi, E. Noohi, S. Parastegari and M. Ẑefran, "Grasp taxonomy based on force distribution." Robot and Human Interactive Communication (RO-MAN), 2016 25th IEEE International Symposium on. IEEE, 2016.
- E. Noohi, S. Parastegari and M. Ẑefran, "Computational model for dyadic and bimanual reaching movements." World Haptics Conference (WHC), IEEE 2015.
- E. Noohi, H. Moradi, S. Parastegari and M. Nili Ahmadabadi, "Object Manipulation Using Unlimited Rolling Contacts: 2-D Kinematic Modeling and Motion Planning." IEEE Transactions on Robotics 31.3 (2015): 790-797.
- E. Noohi, S. Parastegari and M. Ẑefran, "Using monocular images to estimate interaction forces during minimally invasive surgery." Intelligent Robots and Systems (IROS 2014), 2014 IEEE/RSJ International Conference on. IEEE, 2014.
- S. Parastegari, M. Nili Ahmadabadi, E. Noohi and H. Moradi, "Wheeled-tip object manipulation: Modeling and motion planning of throwing an object." Robotics and Biomimetics (ROBIO), 2012 IEEE International Conference on. IEEE, 2012.

Awards

- Wexler fellowship, University of Illinois at Chicago 2012
- The Graduate Student Presenter Award, University of Illinois at Chicago 2016
- The Graduate Student Council Travel Award, University of Illinois at Chicago 2016
- Ranked 3rd among nearly 3000 students in nationwide university entrance exam for master degree in Control, Electrical Engineering 2010
- Silver Medal in Iranian National Olympiad in Physics 2004

Work Experience

- **System Analyst,** Intuitive Surgical Inc., Sunnyvale, CA Since June 2017
- **Research Engineer,** PyroPhase Inc., Chicago, IL May 2014 - May 2017
- **Simulation Engineer Intern,** Intuitive Surgical Inc., Sunnyvale, CA Summer 2016
- **Research Engineer Intern,** Intuitive Surgical Inc., Sunnyvale, CA Summer 2015
- **Research Engineer Intern,** CNH Industrial, Burr Ridge, IL Summer 2014

Teaching Experience

- **Lecturer,** ECE 452: Robotics, Algorithms and Control. Fall 2016
  University of Illinois at Chicago
- **Lecturer,** ECE 350: Principles of Automatic Control. Fall 2015
  University of Illinois at Chicago